


# Nonlinear transient response of rough symmetric two lobe hole entry hybrid journal bearing system

Journal of Vibration and Control  
1–30  
© The Author(s) 2015  
Reprints and permissions:  
sagepub.co.uk/journalsPermissions.nav  
DOI: 10.1177/1077546315575831  
jvc.sagepub.com  


Satish C Sharma<sup>1</sup> and Prashant B Kushare<sup>2</sup>

## Abstract

The present paper describes the effect of surface roughness orientation pattern on the nonlinear transient response of symmetric two lobe capillary compensated hole entry hybrid journal bearing. Nonlinear equations of motion have been solved with the Runge-Kutta method. The stability of the journal bearing system has been studied by obtaining the journal center motion trajectories. The results of the study reveal that the surface roughness pattern significantly changes the stability of capillary compensated two lobe hole entry hybrid journal bearing. Hence, from the bearing stability point of view, a proper selection of the surface roughness pattern and bearing geometry is essential.

## Keywords

Hybrid journal bearing, capillary, nonlinear, two lobe, roughness, stability

## 1. Introduction

Multilobe journal bearings are extensively used to support rotating machinery operating at high speed in many engineering applications as it provides improved dynamic characteristics and better anti-whirl characteristics. The ability of journal bearing to suppress whirl is of prime importance from the stability point of view and also for successful operation of rotary machines. As a consequence of this, many configurations of multilobe journal bearing have been designed and developed by many bearing designers. Owing to this, in recent times, many studies related to multilobe hydrodynamic and hybrid journal bearings have been reported in literature (Pinkus, 1956; Schuller, 1971; Goenka and Booker, 1983; Bouyer et al., 2007; Ghosh and Satish, 2003; Ghosh and Nagraj, 2004; Phalle et al., 2011; Sharma et al., 2012; Kushare and Sharma, 2013).

Even though the advancement in micro finishing processes, surfaces that are found unsatisfactory from the standpoint of quality of surface polishing. It is revealed that the bearing surface remains rough at a microscopic scale. The roughness of this surface is equal to the order of the fluid-film thickness. As a result of this, the bearing response gets changed. Several studies pertaining to the influence of surface roughness on the performance characteristics of

hydrodynamic journal bearings and hybrid journal bearings have been reported in the literature (Christensen, 1969; Patir and Cheng, 1978, 1979; Ramesh et al., 1995; Turaga et al., 1999, 2000; Lin, 2007; Jagadeesha et al., 2012; Fayolle and Childs, 1999; Nagaraju et al., 2002, 2007; Basavaraja et al., 2009). A stochastic model for random rough surface has been developed by Christensen and Tonder (1973). They studied the effect of longitudinal and transverse roughness on the bearing performance. Patir and Cheng (1978, 1979) developed an average flow model to incorporate the roughness effect in the analysis of journal bearing. Average flow model of Patir and Cheng has been extensively used by many bearing researchers (Ramesh et al., 1995; Nagaraju et al., 2002, 2007; Basavaraja et al., 2009) to analyze the influence of surface irregularities. Many studies

<sup>1</sup>Department of Mechanical and Industrial Engineering, Tribology Laboratory, Indian Institute of Technology, Roorkee, India

<sup>2</sup>Mechanical Engineering Department, K.K.Wagh Institute of Engineering Education and Research, Nashik, India

Received: 15 April 2014; accepted: 18 January 2015

## Corresponding author:

Prashant B Kushare, Mechanical Engineering Department, K.K.Wagh Institute of Engineering Education and Research, Nashik, 422003, India.  
Email: pbkushare@gmail.com

have been reported in the literature (San Andres, 1990; Fayolle and Childs, 1999; Nagaraju et al., 2007; Basavaraja et al., 2009) which concerns about the influence of surface roughness on the performance of hybrid journal bearings. A theoretical investigation on hybrid journal bearing by varying the effective depth of roughness was carried out by San Andres (1990). Nagaraju et al. (2007) studied the combined influence of roughness pattern nonlinear behavior of the lubricant on the performance characteristics of circular non recessed hybrid journal bearing. The results of their study indicates that the roughness orientation pattern and non-Newtonian lubricant have significant influence on threshold speed margin. Recently, a theoretical study on effect of surface roughness on misaligned 2-lobe hole-entry hybrid journal bearing was carried out by Basavaraja et al. (2009).

The dynamic performance characteristics of rotary bearing system play a significant role in the stability of a journal bearing system. To avoid the metal-to-metal contact in bearing system and the failure of the rotating systems at the design stage, the dynamic behavior of the bearing system must be accurately predicted. As a consequence of this, many studies concerning the prediction of bearing system stability have been reported in the literature. (Sinhasan and Goyal, 1995; Newkirk and Taylor, 1925; Leonard and Rowe, 1973; Choy et al., 1992; Ramesh et al., 1995; Turaga et al., 1999, 2000; Lin, 2007; Jagadeesha et al., 2012; Malik et al., 1989; Khonsari, 1990; Wang et al., 2012; Pang et al., 1993; San Andres, 1997; Yoshimoto and Kikuchi, 1999; Kushare and Sharma, 2014). The existence of stable behavior in the unstable region was determined by utilizing the linearized and non linearized analysis of hydrodynamic journal bearing systems are reported by many authors in their theoretical and experimental work (Newkirk and Lewis, 1925; Leonard and Rowe, 1973; Lund, 1987; Malik et al., 1989; Choy et al., 1992; Ramesh et al., 1995; Sinhasan and Goyal, 1995; Turaga et al., 1999, 2000; Lin, 2007; Jagadeesha et al., 2012). In 1925, the first experimental study to investigate the rotor dynamic instability in hydrodynamic journal bearings was carried out by Newkirk and Taylor (1925). They reported that the action of oil film has an important role in occurrence of instability and termed it as oil whirl. Lund (1987) introduced the use of critical mass to study the stability and nonlinear motion of the journal. Choy et al. (1992) studied the non-linear characteristics and their effects on the transient response of a plain journal bearing. Sinhasan and Goyal (1995) reported the transient analysis of two-lobe journal bearings lubricated with non-Newtonian lubricant. Ramesh et al. (1995) studied the influence of surface roughness and temperature on the stability of a submerged oil journal bearing by using a

time-transient non-linear analysis. it was reported that the isotropic roughness pattern have more effect on bearing stability with respect to different aspect ratios. Turaga et al. (2000) presented the non-linear transient stability analysis of two symmetric hydrodynamic bearings with rough surfaces. It was reported that the transverse roughness pattern has a high margin of stability than the isotropic roughness. Malik et al. (1989) carried out a series of theoretical investigations concerned with the transient response of a journal in short bearings. The stability margin expressed in terms of critical speed or critical mass of the journal was obtained using the conventional linearized theory. An assessment of a linearized system stability chart was carried out by delineating the motion of an accelerating or decelerating journal. Lin (2007) investigated the effects of isotropic surface roughness on a short journal-bearing system to address limit cycle motion by applying the Hopf bifurcation theorem and Christensen stochastic theory. The result of study indicates that the isotropic roughness predicts enlarged size of limit cycle in motion. Further, Jagadeesha et al. (2012) presented the influence of 3D surface roughness patterns on dynamically loaded journal bearing operating with non-Newtonian lubricant. The results of their study found that the bearing transient response is significantly altered because of a change in roughness orientation pattern. A small number of transient response studies of hydrostatic bearings have also been reported in the literature (Leonard and Rowe, 1973; Pang et al., 1993; San Andres, 1997; Yoshimoto and Kikuchi, 1999; Kushare and Sharma, 2014). The theoretical and experimental work of Leonard and Rowe (1973) highlights the mechanism of whirl instability in hydrodynamic bearings by showing how the hydrostatic stiffness raises the frequency of whirl onset. San Andres (1997) compared a linear and non-linear transient response of recessed hydrostatic journal bearing for varieties of external loads. The equations of motion were solved by taking into account turbulence and thermal energy transport. A stability study of two lobe symmetric whole entry worn hybrid journal bearing by using nonlinear analysis was carried out by Kushare and Sharma (2014). They stated that the wear defect deteriorates the bearing stability when operated with non-Newtonian lubricant. The literature review indicates that the values of stability parameters obtained from non-linear analysis provide a higher value of stability margin when compared to linear analysis. However, in actual conditions non-linearities are present in the bearing; linear theory can provide grossly erroneous prediction of bearing system stability quantitatively and qualitatively (Malik et al., 1989; Ramesh et al., 1995; Sinhasan and Goyal, 1995; Turaga et al., 2000; Jagadeesha et al., 2012). A thorough scan of the

literature reveals that the studies related to the non-linear journal motion trajectories of rough hydrodynamic journal bearings are quite exhaustive (Malik et al., 1989; Ramesh et al., 1995; Sinhasan and Goyal, 1995; Turaga et al., 1999; Jagadeesha et al., 2012) and indicates that surface roughness have a substantial influence on stability of journal bearing systems. Therefore, from stability point of view, to envisage the correct response of journal motions, the influence of roughness pattern parameters and nonlinear model of journal motion trajectories must be considered in the analysis. Moreover, in published literature; no study has yet been reported for the nonlinear transient

response of a rough symmetric 2-lobe non-recessed hybrid journal bearing systems. Therefore, a detailed transient response study for symmetric 2-lobe non-recessed hybrid journal bearing system have been carried out for the qualitative assessment of bearing stability response. The most generally used multilobe journal bearing configuration, i.e. two lobe non recessed journal bearing system is shown in Figure 1.

## 2. Analysis

The average Reynold's equation governing the flow of an isoviscous lubricant field in the clearance space of a

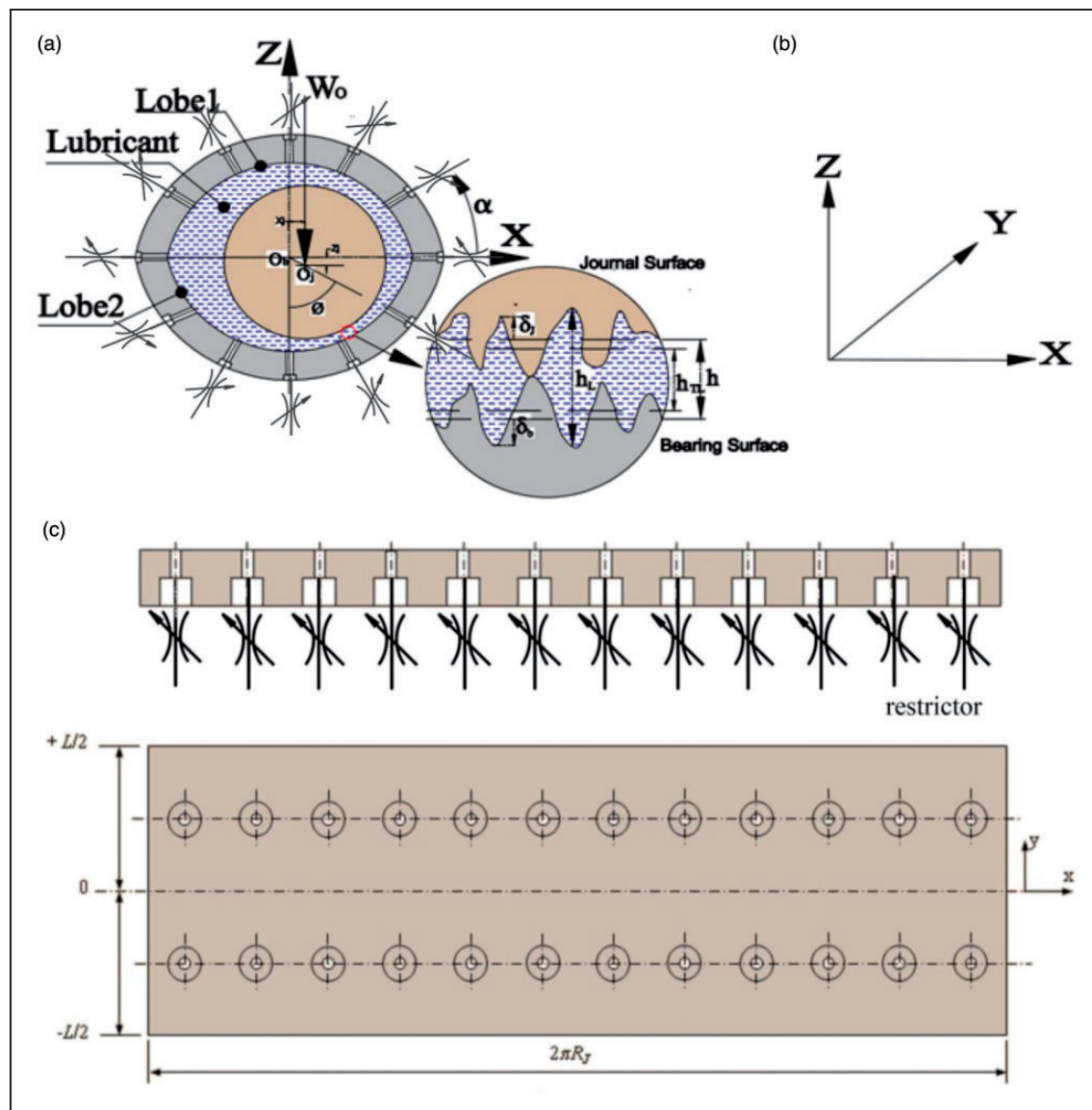


**Figure 1.** Schematic diagram of symmetric two lobe non recessed journal bearing system.

rough journal bearing is written in non-dimensional form as (Dowson, 1962; Patir and Cheng, 1979; Ramesh et al., 1995; Nagaraju et al., 2002)

$$\frac{\partial}{\partial \alpha} \left( \phi_{xL} \frac{\bar{h}^3}{12} \frac{\partial \bar{p}}{\partial \alpha} \right) + \frac{\partial}{\partial \beta} \left( \phi_{yL} \frac{\bar{h}^3}{12} \frac{\partial \bar{p}}{\partial \beta} \right) = \frac{\Omega}{2} \frac{\partial \bar{h}_{TL}}{\partial \alpha} + \frac{\Omega}{2\Lambda} \frac{\partial \phi_{sL}}{\partial \alpha} + \frac{\partial \bar{h}_{TL}}{\partial \tau} \quad (1)$$

where,  $\phi_{xL}$ ,  $\phi_{yL}$  and  $\phi_{sL}$  are the pressure flow factors and shear flow factor respectively and have been computed as reported in Sharma and Kushare (2015).

$\Lambda$  is surface roughness parameter and defined as  $\Lambda = c/\sigma$ , where  $\sigma$  = rms value of the combined surface roughness and is given by  $\sigma = \sqrt{\sigma_b^2 + \sigma_j^2}$ . Where  $\sigma_b$  = rms value of bush surface roughness and  $\sigma_j$  = rms value of journal surface roughness.

### 2.1. Fluid film thickness

The geometry of a symmetric two lobe non recessed hybrid journal bearing is shown in Figure 1. The fluid-film thickness expression ( $\bar{h}$ ) for lobed bearing is written as (Ghosh and Satish, 2003; Phalle et al., 2011; Sharma et al., 2012)

$$\bar{h} = \frac{1}{\delta} - (\bar{X}_j + \bar{x} - \bar{X}_L^i) \cos \alpha - (\bar{Z}_j + \bar{z} - \bar{Z}_L^i) \sin \alpha \quad (2)$$

where,  $\delta$  is the offset factor which specifies the non-circularity of the bearing geometry and is defined as the ratio of clearance due to circumscribed circle on the bearing ( $C_1$ ) to the clearance due to inscribed circle on the bearing ( $C_2$ ).

In the present work, the partial and fully lubricated regions are characterized as the region where  $\Lambda \bar{h} < 3$  and  $\Lambda \bar{h} \geq 3$  respectively (Patir and Cheng, 1978; Ramesh et al., 1995; Nagaraju et al., 2002; Basvaraj et al., 2009). Using these conditions, the expression for average fluid-film thickness ( $\bar{h}_{TL}$ ) is expressed as (Nagaraju et al., 2002)

$$\bar{h}_{TL} = \begin{cases} \frac{\bar{h}}{2} \left( 1 + \operatorname{erf} \left( \frac{\Lambda \bar{h}}{\sqrt{2}} \right) \right) + \frac{1}{\Lambda \sqrt{2\pi}} e^{-(\Lambda \bar{h})^2/2} & \text{for } \Lambda \bar{h} < 3 \\ \bar{h} & \text{for } \Lambda \bar{h} \geq 3 \end{cases} \quad (3)$$

### 2.2. Finite element formulation

The lubricant flow field is discretized by using four-noded quadrilateral isoparametric elements. The pressure variation is assumed to vary linearly over an element and is expressed as (Sinhasan and Goyal, 1995;

Nagaraju et al., 2002; Phalle et al., 2011; Kushare and Sharma, 2013)

$$\bar{p} = \sum_{j=1}^{n_f} \bar{p}_j N_j \quad (4)$$

Using Galerkin's orthogonality conditions the global system of equation is obtained as below

$$[\bar{F}]\{\bar{P}\} = \{\bar{Q}\} + \Omega\{\bar{R}_H\} + \bar{X}_J\{\bar{R}_x\} + \bar{Z}_J\{\bar{R}_z\} \quad (5)$$

where,

$[\bar{F}]$  = assembled fluidity matrix,

$\{\bar{p}\}$  = nodal pressure vector,

$\{\bar{Q}\}$  = nodal flow vector,

$\{\bar{R}_H\}$  = column vectors due to hydrodynamic terms and

$\{\bar{R}_x\}$ ,  $\{\bar{R}_z\}$  = global right hand side vector due to journal center velocities.

The coefficients of the matrices in the above equation for an  $e$ th element are defined as

$$\bar{F}_{ij}^e = \int \int_{A_e} \frac{\bar{h}^3}{12} \left[ \phi_{xL} \frac{\partial N_i}{\partial \alpha} \frac{\partial N_j}{\partial \alpha} + \phi_{yL} \frac{\partial N_i}{\partial \beta} \frac{\partial N_j}{\partial \beta} \right] d\alpha d\beta \quad (5.1)$$

$$\bar{Q}_i^e = \int_{\Gamma^e} \left\{ \frac{\bar{h}^3}{12} \left( \phi_{xL} \frac{\partial \bar{p}}{\partial \alpha} + \phi_{xL} \frac{\partial \bar{p}}{\partial \beta} \right) + \frac{\Omega}{2} \left( \bar{h}_{TL} + \frac{\phi_s}{\Lambda} \right) \right\} N_i d\Gamma^e \quad (5.2)$$

$$\bar{R}_{Hi}^e = \frac{1}{2} \int \int_{A_e} \left( \bar{h}_{TL} + \frac{\phi_{sL}}{\Lambda} \right) \frac{\partial N_i}{\partial \alpha} d\alpha d\beta \quad (5.3)$$

$$\bar{R}_{Xj}^e = \int \int_{A_e} \frac{1}{2} \left[ 1 + \operatorname{erf} \left( \frac{\Lambda \bar{h}}{\sqrt{2}} \right) \right] N_i \cos \alpha d\alpha d\beta \quad (5.4)$$

$$\bar{R}_{Zi}^e = \int \int_{A_e} \frac{1}{2} \left[ 1 + \operatorname{erf} \left( \frac{\Lambda \bar{h}}{\sqrt{2}} \right) \right] N_i \sin \alpha d\alpha d\beta \quad (5.5)$$

### 2.3. Restrictor flow equation

The equation of lubricant flow through a capillary restrictor in the non-dimensional form is expressed as (Basvaraj et al., 2009)

$$\bar{Q}_R = \bar{C}_{s2}(1 - \bar{p}_c) \quad (6)$$

### 2.4. Boundary conditions

The Reynold's equation of the lubricant flow field has been solved in conjunction with capillary restrictor flow equation by using the following associated boundary

conditions (Nagaraju et al., 2002; Kushare and Sharma, 2014)

1. Nodes situated on the external edges of the bearing have zero relative pressure with respect to ambient temperature  $\bar{p}|_{\beta=\mp 1.0}=0.0$ ;
2. Nodes on hole have equal pressure;
3. Flow of lubricant through the restrictor is equal to the bearing input flow;
4. At the trailing edge of the positive region, the pressure gradient is zero.

$$\bar{p} = \frac{\partial \bar{p}}{\partial \alpha} = 0.0 \text{ (Reynolds boundary Condition)}$$

## 2.5. Stability parameters

For a very small disturbance from the equilibrium position, the fluid-film forces in the journal are considered as linear functions of the displacements and the velocity vectors. The disturbed motion of the journal in the form of the linearized equation of motion is expressed as (Sinhasan and Goyal, 1995; Malik et al., 1989; Kushare and Sharma, 2014)

$$[\bar{M}_J]\{\ddot{\bar{X}}_J\} + [\bar{C}]\{\dot{\bar{X}}_J\} + [\bar{S}]\{\bar{X}_J\} = 0 \quad (7)$$

The above equation of motion can be written in matrix form as

$$\begin{bmatrix} \bar{M}_J & 0 \\ 0 & \bar{M}_J \end{bmatrix} \begin{Bmatrix} \ddot{\bar{X}}_J \\ \ddot{\bar{Z}}_J \end{Bmatrix} + \begin{bmatrix} \bar{C}_{xx} & \bar{C}_{xz} \\ \bar{C}_{zx} & \bar{C}_{zz} \end{bmatrix} \begin{Bmatrix} \dot{\bar{X}}_J \\ \dot{\bar{Z}}_J \end{Bmatrix} + \begin{bmatrix} \bar{S}_{xx} & \bar{S}_{xz} \\ \bar{S}_{zx} & \bar{S}_{zz} \end{bmatrix} \begin{Bmatrix} \bar{X}_J \\ \bar{Z}_J \end{Bmatrix} = \begin{Bmatrix} 0 \\ 0 \end{Bmatrix} \quad (8)$$

The characteristic polynomial equation for the two-degree of freedom system is a quadratic equation of the following form

$$a_1 s^4 + a_2 s^3 + a_3 s^2 + a_4 s + a_5 = 0 \quad (9)$$

$$a_1 = 1 > 0 \quad (9.1)$$

$$a_2 = \frac{1}{\bar{M}_J} [\bar{C}_{xx} + \bar{C}_{zz}] > 0 \quad (9.2)$$

$$a_3 = \frac{1}{\bar{M}_J^2} [\bar{C}_{xx}\bar{C}_{zz} + \bar{M}_J[\bar{S}_{xx} + \bar{S}_{zz}] - \bar{C}_{xz}\bar{C}_{zx}] > 0 \quad (9.3)$$

$$a_4 = \frac{1}{\bar{M}_J^2} [\bar{S}_{xx}\bar{C}_{zz} + \bar{S}_{zz}\bar{C}_{xx} - \bar{S}_{xz}\bar{C}_{zx} - \bar{S}_{zx}\bar{C}_{xz}] > 0 \quad (9.4)$$

$$a_5 = \frac{1}{\bar{M}_J^2} [\bar{S}_{xx}\bar{S}_{zz} - \bar{S}_{xz}\bar{S}_{zx}] > 0 \quad (9.5)$$

Using the characteristic equation 9 and Routh's criteria, the stability parameter of bearing system is expressed in terms of critical mass ( $\bar{M}_c$ ) and threshold speed.

**2.5.1. Critical mass ( $\bar{M}_c$ ).** Critical mass ( $\bar{M}_c$ ) in nondimensional form is defined as

$$\bar{M}_c = \frac{\bar{G}_1}{\bar{G}_2 - \bar{G}_3} \quad (10)$$

$$\bar{G}_1 = [\bar{C}_{xx}\bar{C}_{zz} - \bar{C}_{zx}\bar{C}_{xz}] \quad (10.1)$$

$$\bar{G}_2 = \frac{[\bar{S}_{xx}\bar{S}_{zz} - \bar{S}_{xz}\bar{S}_{zx}][\bar{C}_{xx} + \bar{C}_{zz}]}{[\bar{S}_{xx}\bar{C}_{zz} + \bar{S}_{zz}\bar{C}_{xx} - \bar{S}_{xz}\bar{C}_{zx} - \bar{S}_{zx}\bar{C}_{xz}]} \quad (10.2)$$

$$\bar{G}_3 = \frac{[\bar{S}_{xx}\bar{C}_{xx} + \bar{S}_{xz}\bar{C}_{xz} + \bar{S}_{zx}\bar{C}_{zx} + \bar{S}_{zz}\bar{C}_{zz}]}{[\bar{C}_{xx} + \bar{C}_{zz}]} \quad (10.3)$$

**2.5.2. Threshold speed ( $\bar{\omega}_{th}$ ).** Threshold speed ( $\bar{\omega}_{th}$ ) in nondimensional form is expressed as

$$\bar{\omega}_{th} = [\bar{M}_c / \bar{F}_0]^{1/2} \quad (11)$$

where,  $\bar{F}_0$  is resultant fluid-film force or reaction ( $\frac{\partial \bar{h}}{\partial t} = 0$ )

## 2.6. Linear model for motion trajectories

The out of balance forces  $\Delta F_x$  and  $\Delta F_z$  are developed when the journal is disturbed from its static equilibrium position. These forces depend on the instantaneous position and velocity of the journal center. Mathematically, the equation of disturbed motion of the journal is written as (Sinhasan and Goyal, 1995; Malik et al., 1989)

$$[\bar{M}_J] \begin{Bmatrix} \ddot{\bar{X}}_J \\ \ddot{\bar{Z}}_J \end{Bmatrix} = \begin{Bmatrix} \Delta \bar{F}_x(\bar{X}_J, \bar{Z}_J, \dot{\bar{X}}_J, \dot{\bar{Z}}_J) \\ \Delta \bar{F}_z(\bar{X}_J, \bar{Z}_J, \dot{\bar{X}}_J, \dot{\bar{Z}}_J) \end{Bmatrix} \quad (12)$$

where  $[\bar{M}_J]$  is a diagonal mass matrix,  $\ddot{\bar{X}}_J$  and  $\ddot{\bar{Z}}_J$  are the components of acceleration in  $x$  and  $z$  directions respectively.



Thus equation (12) may be written in terms of stiffness and damping coefficients at any time  $\bar{t}$  (Sinha and Goyal, 1995; Malik et al., 1989)

$$\begin{bmatrix} \bar{M}_J & 0 \\ 0 & \bar{M}_J \end{bmatrix} \begin{Bmatrix} \ddot{\bar{X}}_J \\ \ddot{\bar{Z}}_J \end{Bmatrix}_{|\bar{t}} = \begin{Bmatrix} \Delta \bar{F}_x \\ \Delta \bar{F}_z \end{Bmatrix}_{|\bar{t}} = - \begin{bmatrix} \bar{S}_{xx} & \bar{S}_{xz} & \bar{C}_{xx} & \bar{C}_{xz} \\ \bar{S}_{zx} & \bar{S}_{zz} & \bar{C}_{zx} & \bar{C}_{zz} \end{bmatrix} \begin{Bmatrix} \bar{X}_J \\ \bar{Z}_J \\ \dot{\bar{X}}_J \\ \dot{\bar{Z}}_J \end{Bmatrix}_{|\bar{t}} \quad (12.1)$$

where the subscript  $\bar{t}$  refers to the instantaneous values. The stiffness and damping coefficients ( $\bar{S}_{xx}$ ,  $\bar{S}_{xz}$ ,  $\bar{S}_{zx}$ ,  $\bar{S}_{zz}$ ,  $\bar{C}_{xx}$ ,  $\bar{C}_{xz}$ ,  $\bar{C}_{zx}$  and  $\bar{C}_{zz}$ ) are evaluated at the static equilibrium position of the journal center and expressed as

$$\begin{bmatrix} \bar{S}_{xx} & \bar{S}_{xz} \\ \bar{S}_{zx} & \bar{S}_{zz} \end{bmatrix} = - \int_{\Omega} \begin{bmatrix} \bar{p}_{\bar{X}_j} \sin \theta & \bar{p}_{\bar{X}_j} \sin \theta \\ \bar{p}_{\bar{Z}_j} \cos \theta & \bar{p}_{\bar{Z}_j} \cos \theta \end{bmatrix} \partial \Omega \quad (12.2)$$

$$\begin{bmatrix} \bar{C}_{xx} & \bar{C}_{xz} \\ \bar{C}_{zx} & \bar{C}_{zz} \end{bmatrix} = - \int_{\Omega} \begin{bmatrix} \bar{p}_{\dot{\bar{X}}_j} \sin \theta & \bar{p}_{\dot{\bar{X}}_j} \sin \theta \\ \bar{p}_{\dot{\bar{Z}}_j} \cos \theta & \bar{p}_{\dot{\bar{Z}}_j} \cos \theta \end{bmatrix} \partial \Omega \quad (12.3)$$

To obtain  $\bar{x}_j$ ,  $\bar{z}_j$ ,  $\dot{\bar{x}}_j$  and  $\dot{\bar{z}}_j$  which gives the locus of the journal, equation (12.1) is integrated for certain initial disturbance  $\bar{X}_j$ ,  $\bar{Z}_j$ ,  $\dot{\bar{X}}_j$  and  $\dot{\bar{Z}}_j$ .

### 2.7. Nonlinear model for motion trajectories

The nonlinear equation of disturbed motion of the journal in terms of the instantaneous fluid-film force

components  $\bar{F}_x$  and  $\bar{F}_z$  are written as (Sinha and Goyal, 1995; Kushare and Sharma, 2014)

$$\bar{M}_J \ddot{\bar{X}}_j = \Delta \bar{F}_x(\bar{X}, \bar{Z}, \dot{\bar{X}}, \dot{\bar{Z}}) \quad (13.1)$$

$$\bar{M}_J \ddot{\bar{Z}}_j = \Delta \bar{F}_z(\bar{X}, \bar{Z}, \dot{\bar{X}}, \dot{\bar{Z}}) \quad (13.2)$$

At any time  $\bar{t}$ , the nonlinear equation of motion can be written as in matrix form

$$\begin{bmatrix} \bar{M}_J & 0 \\ 0 & \bar{M}_J \end{bmatrix} \begin{Bmatrix} \ddot{\bar{X}}_j \\ \ddot{\bar{Z}}_j \end{Bmatrix}_{|\bar{t}} = \begin{Bmatrix} \Delta \bar{F}_x \\ \Delta \bar{F}_z \end{Bmatrix}_{|\bar{t}} = \begin{Bmatrix} \bar{F}_x - \bar{F}_{x0} \\ \bar{F}_z - \bar{F}_{z0} \end{Bmatrix}_{|\bar{t}} \quad (13.3)$$

where  $\bar{F}_{x0}$  and  $\bar{F}_{z0}$  are the fluid-film force components of the static equilibrium position and  $\bar{F}_x$  and  $\bar{F}_z$  are fluid-film force components. At each time step  $\bar{F}_x$  and  $\bar{F}_z$  are evaluated after establishing the pressure field corresponding to the position of the journal. Equation (13.3) is integrated using the fourth order Runge-Kutta method to obtain the nonlinear trajectory.

### 3. Solution scheme

The iterative solution scheme employed for the solution of different governing equations used in the analysis is shown in Figure 2. In unit FLEM, the value of average fluid film thickness ( $\bar{h}_{TL}$ ) at all the nodal points are calculated by using the expression of nominal fluid film thickness of lobed bearing (equation 2). In ROUGHN block, the PFF and SFF unit are used to compute the pressure flow factor ( $\phi_{xL}$ ,  $\phi_{yL}$ ) and shear

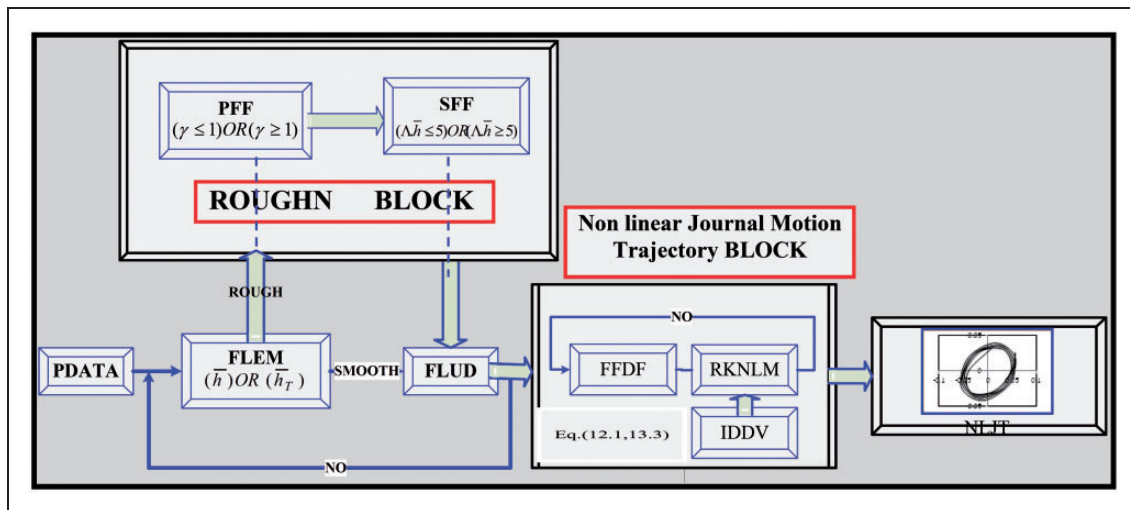


Figure 2. An iterative solution scheme.

**Table 1.** Bearing geometric and operating parameters.

Bearing geometric parameter	Symbol	Bearing type hybrid	Unit
Journal radius	$R_j$	50	mm
Bearing length	$L$	100	mm
Bush thickness	$t_b$	5	mm
Land width ratio	$a_b/L$	0.25	—
Aspect ratio	$\lambda$	1.0	—
Variance ratio	$\bar{V}_{rj}$	0.5	—
Surface roughness parameter	$\Lambda$	4	—
Symmetric bearing configuration	No. of rows (n)	02	—
	No. of holes per row (k)	12	—
Compensating element	Capillary		—
<i>Lubricant characteristics</i>			
Specific heat	$C_p$	2000	$\text{J kg}^{-1}\text{K}^{-1}$
Density	$\rho_f$	860	$\text{kg m}^{-3}$
Thermal conductivity	$k_f$	0.125	$\text{W m}^{-1}\text{K}^{-1}$
Viscosity (at 40 degree Celsius)	$\mu$	0.02636	Pa s
<i>Operating parameters</i>			
Journal speed	$N$	2500	rpm
External load	$W_o$	22.4	kN
	$\bar{W}_o$	2- 4	—
Supply pressure	$p_s$	$8.96 \times 10^6$	$\text{N m}^{-2}$
Supply temperature	$T_s$	40	$^{\circ}\text{C}$
Ambient temperature	$T_a$	40	$^{\circ}\text{C}$
Restrictor design parameter	$\bar{C}_{s2}$	0.087	—
Offset factor	$(\delta)$	0.80, 1.0, 1.20	—
Surface pattern parameter	$(\gamma)$	1/6, 1 and 6	—

flow factor ( $\phi_{sL}$ ). The solution of Reynolds equation (equation 1) and the capillary restrictor flow equation (equation 6) is obtained by incorporating appropriate boundary conditions (section 2.4). In Unit Fluid, the nodal pressure and velocity components of the lubricant flow field are obtained by solving a global system of equation (equation 5) with desired convergence criteria. In unit RKNLM, fluid film force components are determined using the converged value of nodal pressures. In NLJT unit, by using initial values of disturbances  $\bar{X}$ ,  $\bar{Y}$ ,  $\bar{Z}$  and  $\dot{\bar{Z}}$ , the nonlinear trajectories of journal center motion are obtained by integrating the equation of motion (equations 12, 13.3) using the fourth order Runge-Kutta method.

#### 4. Result and discussions

The journal center motion trajectories for 2-lobe non-recessed hybrid journal bearings have been computed by using non-linear equation of motions and the solution method stated in the earlier section 3. The judiciously selected values of bearing characteristics in

terms of bearing geometric and operating parameters (Sinhasan and Goyal, 1995; Malik et al., 1989; Ghosh and Satish, 2003; Phalle et al., 2011; Nagaraju et al., 2002) as shown in Table 1 have been used in the analysis for the study. In the published literature, as confirmed previously, no nonlinear stability analysis of journal trajectory motion studies is available for a 2-lobe symmetric non-recessed rough bearing. Therefore, in order to establish the validity of developed numeric model, the computed results of the present study have been compared and validated with the already published results of Sinhasan and Goyal (1995) and Ramesh et al. (1995). For the journal motion trajectory study, journal center motion trajectories are plotted for a circular hydrodynamic journal bearing for  $\bar{W}_0 = 2.0$ ,  $\bar{K} = 0.0$  when  $\bar{M}_j = \bar{M}_c$  and are shown in Figure 3. The linear and non-linear journal motion trajectories compare well with the published result (Sinhasan and Goyal, 1995). Further, in the published literature, no results have yet been reported for the case of rough symmetric 2-lobe hole entry hybrid journal bearings.

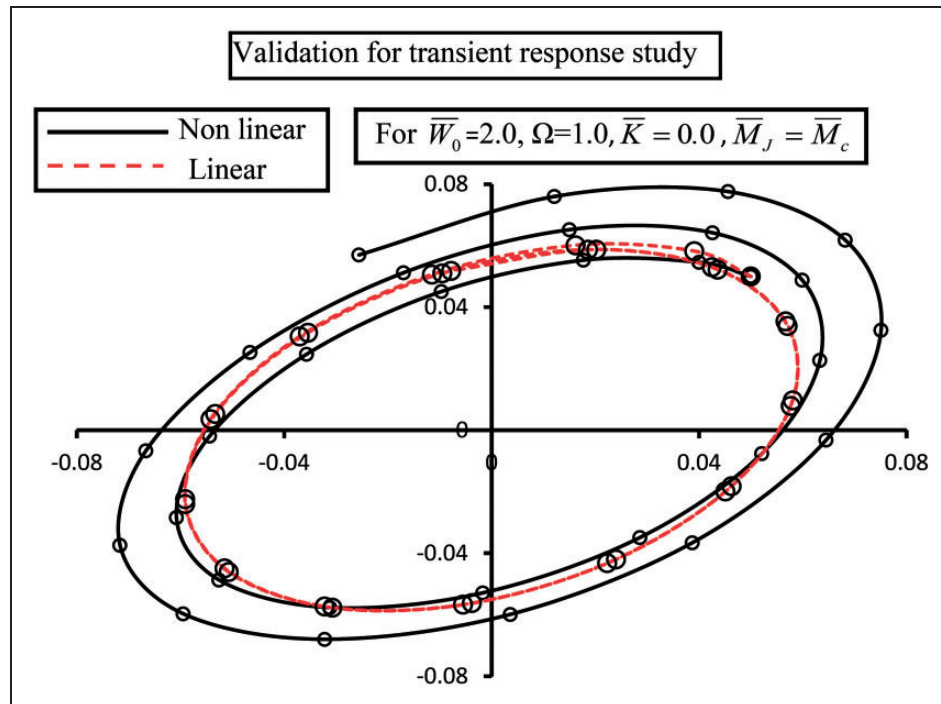


Figure 3. Journal centre motion trajectories for circular hydrodynamic journal bearing.

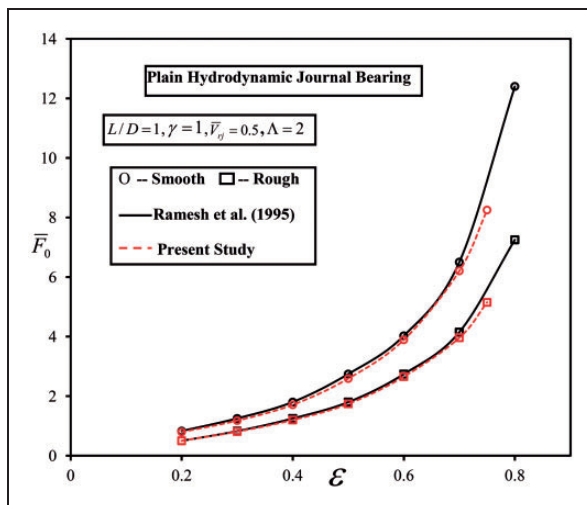


Figure 4. Fluid film reaction ( $\bar{F}_0$ ) with an eccentricity ratio ( $\epsilon$ ).

Therefore, the results are computed for both the plain smooth and rough surface hydrodynamic journal bearing. These results show better agreement with the published results of Ramesh et al. (1995) and presented in Figure 4. The difference in results is observed because of different numerical methods adopted in the studies.

As pointed out earlier, nonlinear transient response generally predicts higher values of stability parameters however, in some of the studies, the linear analysis

reported as the best possible solution of engineering design problems. Therefore, for the sake of clarity, a comparison of stability parameters has been carried out using the linear and non-linear analysis. Stability of two lobe non recessed journal bearing has been studied in terms of stability threshold speed margin and critical journal mass. Further, the nonlinear journal center motion trajectories have been drawn and presented for the different values of surface roughness pattern ( $\gamma$ ) for  $\bar{M}_J = 1.1\bar{M}_c$ ,  $\bar{M}_J = \bar{M}_c$  and  $\bar{M}_J = 0.9\bar{M}_c$ . Surface pattern parameter ( $\gamma$ ) accounts the direction of surface roughness orientation and defined as  $\gamma = \lambda_{0.5x} / \lambda_{0.5y}$  where,  $\lambda_{0.5x}$  and  $\lambda_{0.5y}$  are the autocorrelation lengths of  $x$  profile (circumferential direction) and  $y$  profile (axial direction).

In transversely oriented roughness pattern,  $\lambda_{0.5y} > \lambda_{0.5x}$  thus, surface pattern parameter ( $\gamma$ ) becomes less than one ( $\gamma < 1$ ). Further in isotropic pattern,  $\lambda_{0.5x} = \lambda_{0.5y}$  hence, the value of surface pattern parameter becomes equal to one ( $\gamma = 1$ ). For longitudinally oriented roughness pattern,  $\lambda_{0.5x} > \lambda_{0.5y}$  therefore, the values of surface pattern parameter  $\gamma$  is greater than one (i.e.  $\gamma > 1$ ). The results in terms of stability threshold speed margin and critical journal mass are plotted in Figure 5(a–d) and Figure 6(a–d). The variation of stability threshold speed margin ( $\bar{\omega}_{th}$ ) with respect to an external load ( $\bar{W}_0$ ) for different surface roughness pattern ( $\gamma$ ) is shown in Figure 5(a–d). The nonlinear analysis provides a largest value of threshold



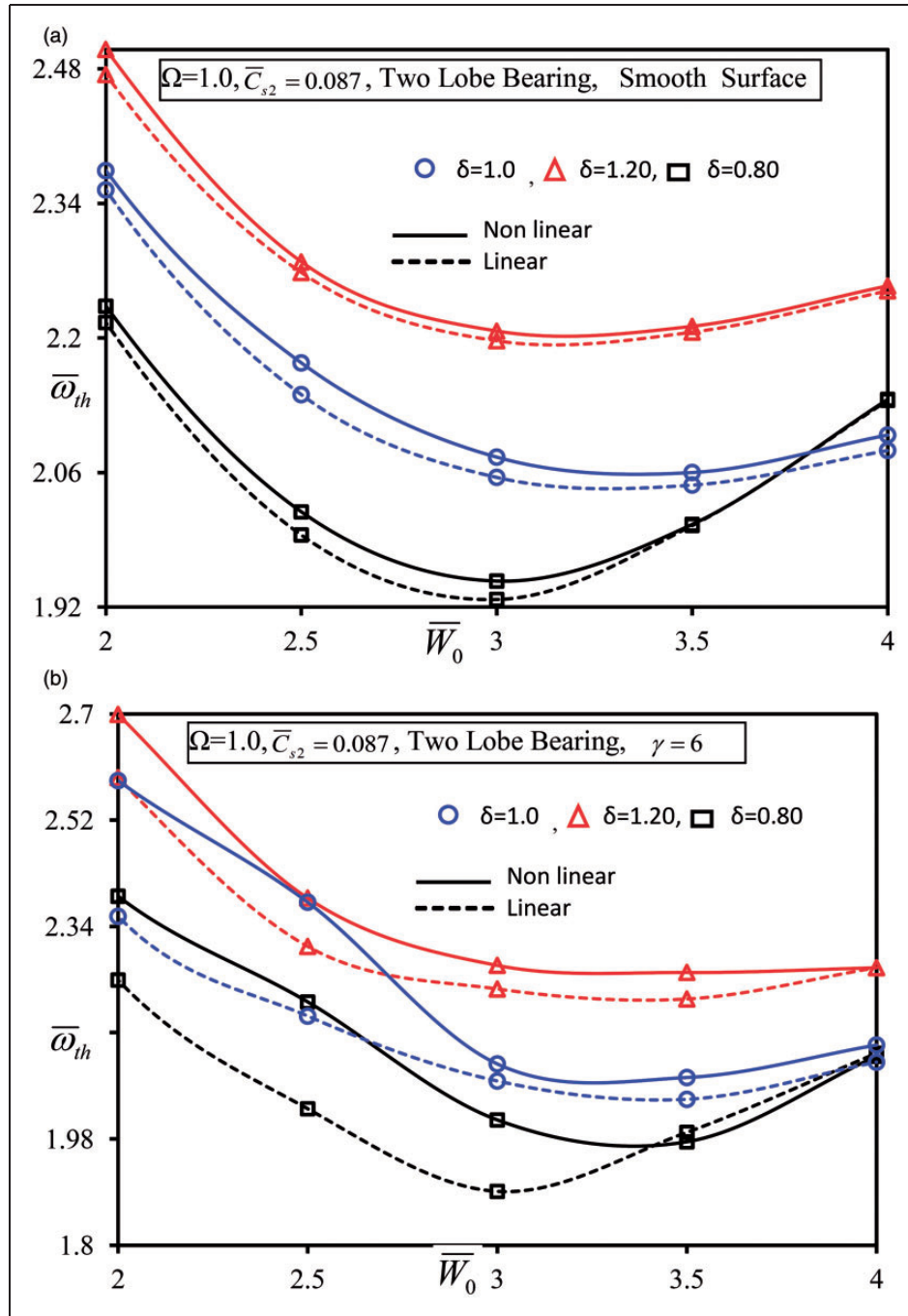


**Figure 5.** (a) Variation of  $\bar{\omega}_{th}$  with respect to  $\bar{W}_0$  for smooth surface; (b) Variation of  $\bar{\omega}_{th}$  with respect to  $\bar{W}_0$  for  $\gamma = 6$ ; (c) Variation of  $\bar{\omega}_{th}$  with respect to  $\bar{W}_0$  for  $\gamma = 1/6$ ; (d) Variation of  $\bar{\omega}_{th}$  with respect to  $\bar{W}_0$  for  $\gamma = 1$ .

speed margin for smooth pattern surface bearing for circular and noncircular 2-lobe symmetric non recessed bearing configurations. Further from Figure 5(a), it may be observed that the threshold speed margin  $\bar{\omega}_{th}$  gets decreased for the lower values of an external load (up to  $\bar{W}_0 = 3.0$ ), and then increased to the higher value of an external load. The influence of the longitudinal

roughness pattern parameter on threshold speed margin is shown in Figure 5(b). For longitudinal roughness pattern, the non-linear analysis shows significant improvement in the value of threshold speed margin ( $\bar{\omega}_{th}$ ) for the value of offset factor  $\delta = 1.20$ ,  $\delta = 1.0$  and  $\delta = 0.80$  whereas the linear analysis has a marginal influence on threshold speed margin ( $\bar{\omega}_{th}$ ) for the value of offset factor  $\delta = 1.0$  and  $\delta = 0.80$ . As shown in Figure 5(c–d), the influence of the transverse and

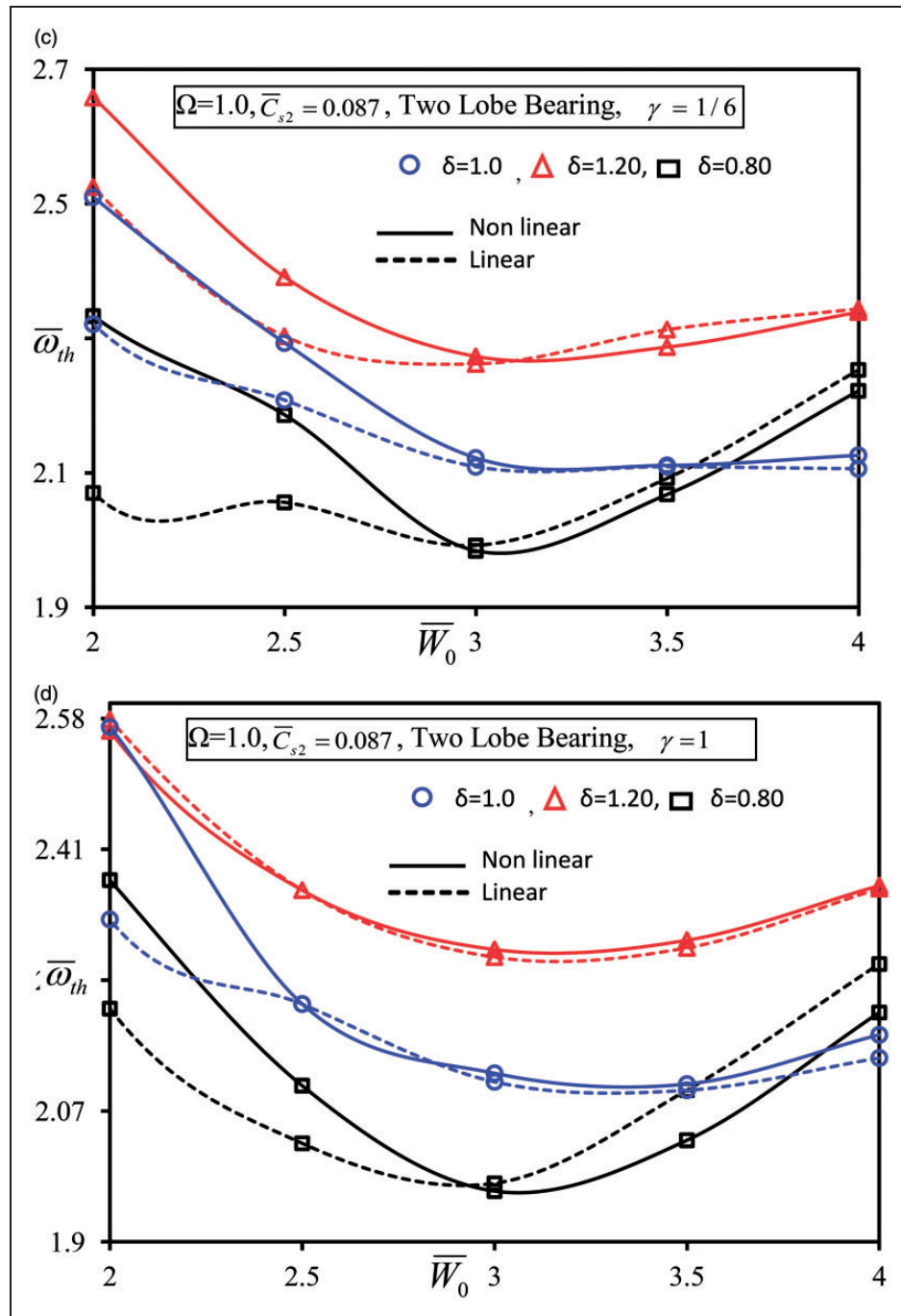
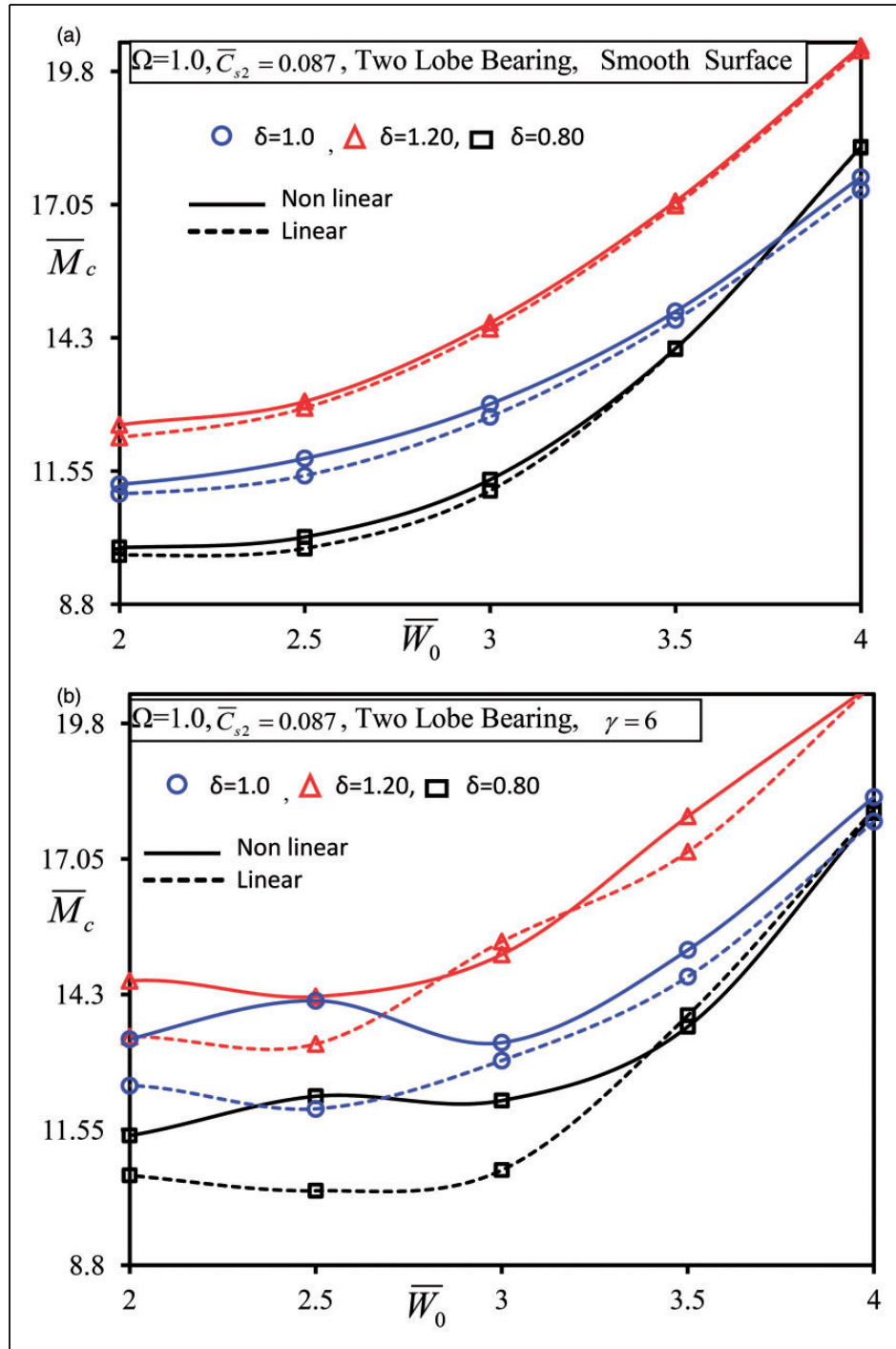


Figure 5. Continued.

isotropic roughness pattern is observed at lower value of an external load ( $\bar{W}_0 \leq 3.0$ ). The nonlinear analysis provides higher value of stability threshold speed margin up to the value of an external load ( $\bar{W}_0 = 3.0$ ) thereafter, the linear analysis shows the significant improvement in stability for circular ( $\delta = 1.0$ ) as well as non circular bearings ( $\delta = 1.20$ ,  $\delta = 0.80$ ). The

nonlinear analysis provides more stability threshold speed margin than the linear analysis. It may also be noticed that the transverse roughness and longitudinal roughness have a propensity to increase the stability of the value of offset factor more than one whereas decreasing trend is observed for isotropic roughness and smooth surface.



**Figure 6.** (a) Variation of  $\bar{M}_c$  with respect to  $\bar{W}_0$  for smooth surface; (b) Variation of  $\bar{M}_c$  with respect to  $\bar{W}_0$  for  $\gamma = 6$ ; (c) Variation of  $\bar{M}_c$  with respect to  $\bar{W}_0$  for  $\gamma = 1/6$ ; (d) Variation of  $\bar{M}_c$  with respect to  $\bar{W}_0$  for  $\gamma = 1$ .

The variation of critical journal mass ( $\bar{M}_c$ ) with respect to an external load is presented in Figure 6(a–d) for the different roughness pattern. The results are computed using linearized equations of motion and non-linearized equation of motion. Figure 6(a) indicates the influence of smooth surface pattern on the

critical journal mass ( $\bar{M}_c$ ) for the values of different offset factor ( $\delta$ ). It may be observed that the smooth surface has a significant effect on the critical journal mass at lower values of external load i.e.  $\bar{W}_0 \leq 3.0$ , and marginal influence at higher loads  $\bar{W}_0 \geq 3.0$ . The nonlinear analysis provides higher value of critical

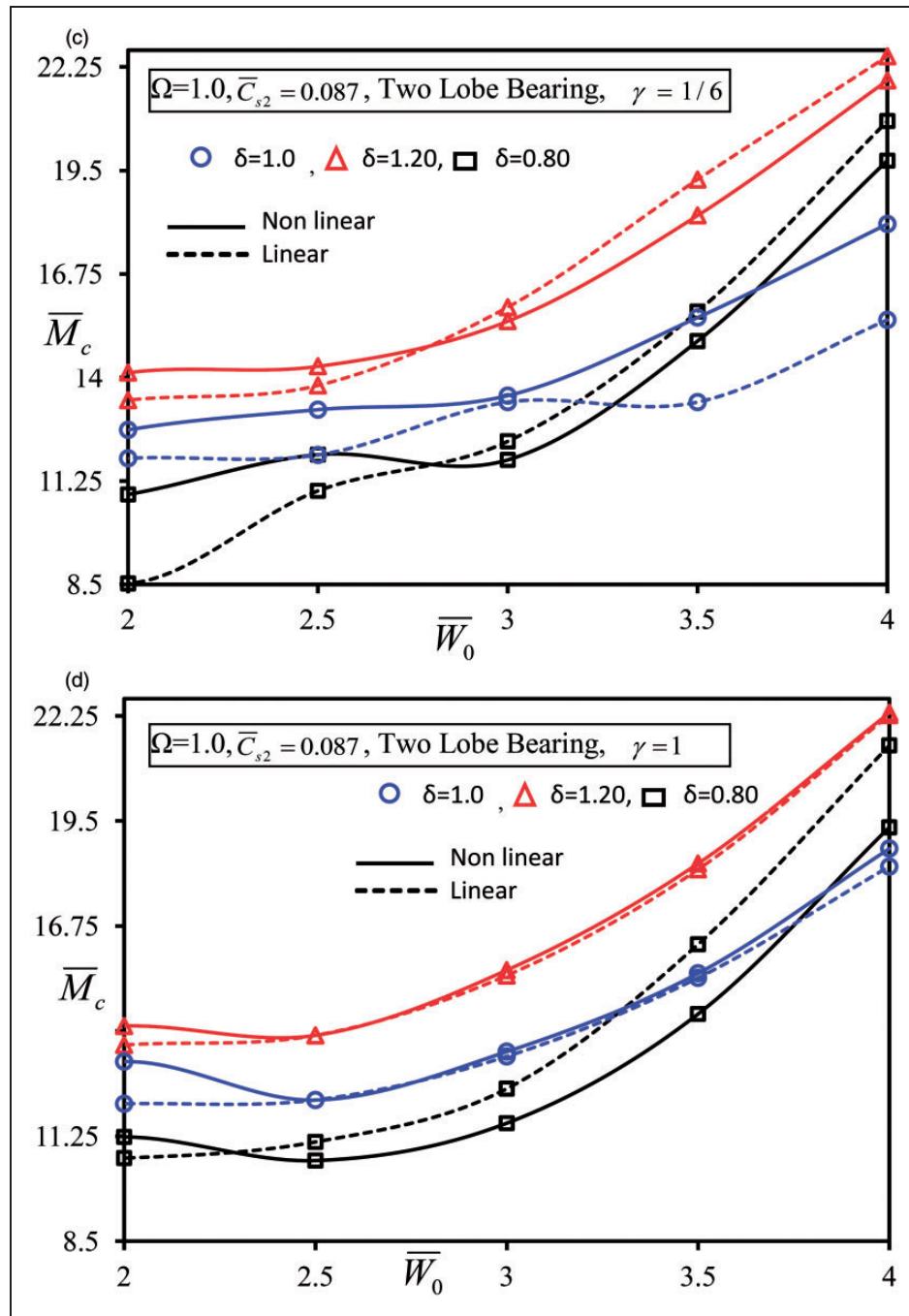
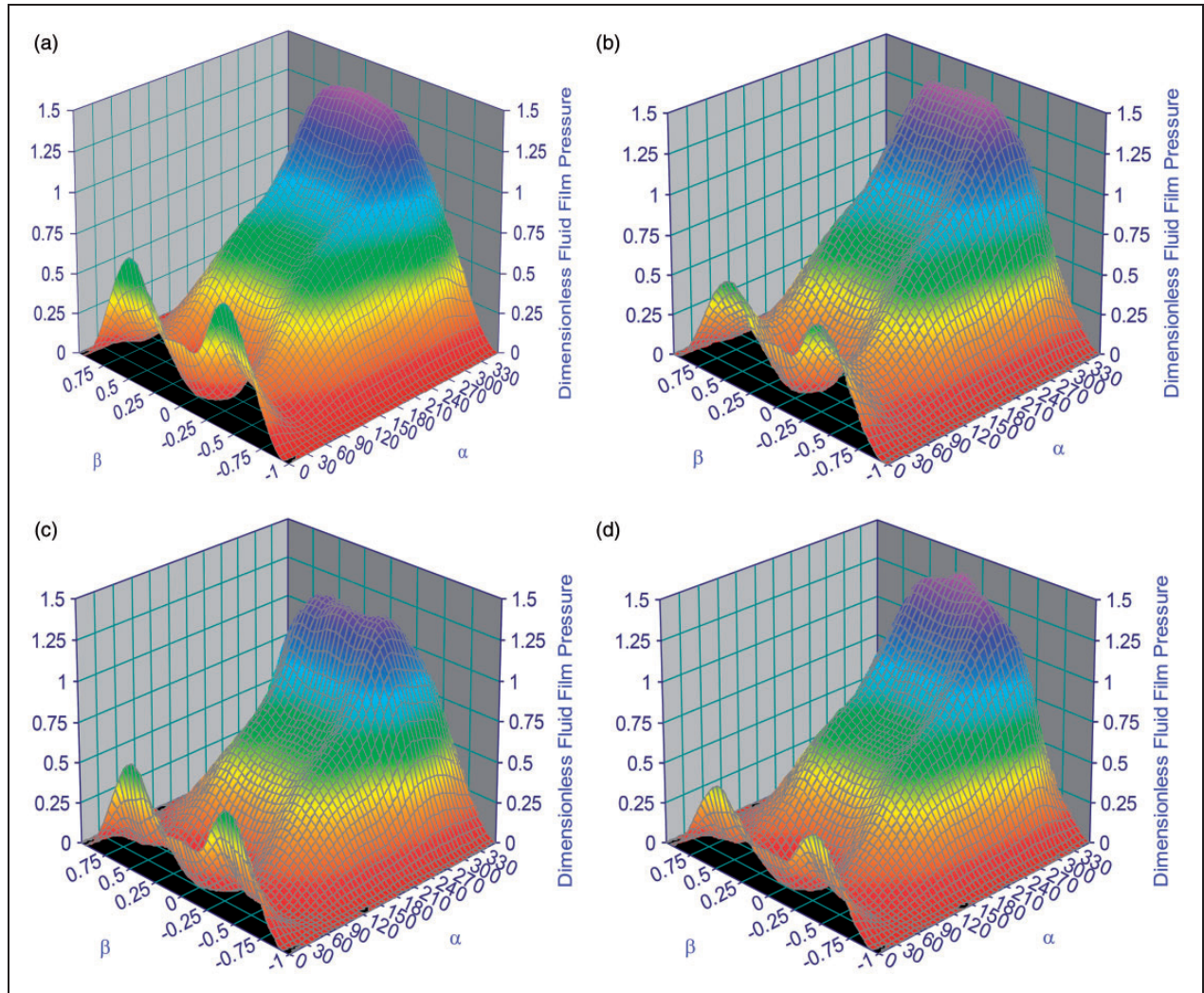


Figure 6. Continued.

journal mass ( $\bar{M}_c$ ) than the linear analysis. As shown in Figure 6(b), the nonlinear analysis provides the largest margin of critical journal mass for the value of the offset factor ( $\delta = 1.20$  and  $\delta = 1.0$ ). Further, it may be revealed that the linear analysis predicts the higher value of critical journal mass at a higher value of external load ( $\bar{W}_0 \geq 3.0$ ) for longitudinal roughness pattern ( $\gamma = 6$ ). Further, from stability point of view, the

margin of linear and nonlinear analysis is far more than any other roughness pattern. Figure 6(c) shows the variation of critical journal mass for transverse roughness pattern ( $\gamma = 1/6$ ). For noncircular journal bearing, the nonlinear analysis provides more stability than the linear analysis at the value of an external load  $\bar{W}_0 \leq 2.5$ . The linear analysis shows significant effect on critical journal mass ( $\bar{M}_c$ ) for the value of external load





**Figure 7.** (a) Linear analysis,  $\Omega = 1.0$ ,  $\bar{C}_{s2} = 0.087$ ,  $\delta = 1.20$ ,  $\gamma = 6$ , Two Lobe Bearing; (b) Non-linear analysis,  $\Omega = 1.0$ ,  $\bar{C}_{s2} = 0.087$ ,  $\delta = 1.20$ ,  $\gamma = 6$ , Two Lobe Bearing; (c) Linear analysis,  $\Omega = 1.0$ ,  $\bar{C}_{s2} = 0.087$ ,  $\delta = 1.20$ ,  $\gamma = 1/6$ , Two Lobe Bearing; (d) Non-linear analysis,  $\Omega = 1.0$ ,  $\bar{C}_{s2} = 0.087$ ,  $\delta = 1.20$ ,  $\gamma = 1/6$ , Two Lobe Bearing; (e) Linear analysis,  $\Omega = 1.0$ ,  $\bar{C}_{s2} = 0.087$ ,  $\delta = 1.20$ ,  $\gamma = 1$ , Two Lobe Bearing; (f) Non-linear analysis,  $\Omega = 1.0$ ,  $\bar{C}_{s2} = 0.087$ ,  $\delta = 1.20$ ,  $\gamma = 1$ , Two Lobe Bearing; (g) Linear analysis,  $\Omega = 1.0$ ,  $\bar{C}_{s2} = 0.087$ ,  $\delta = 1.20$ , Smooth Surface Two Lobe Bearing; (h) Non-linear analysis,  $\Omega = 1.0$ ,  $\bar{C}_{s2} = 0.087$ ,  $\delta = 1.20$ , Smooth Surface, Two Lobe Bearing.

more than  $\bar{W}_0 \geq 2.5$ . The nonlinear and linear analysis results of critical journal mass ( $\bar{M}_c$ ) are presented in Figure 6(d) for different values of offset factor ( $\delta$ ) for isotropic roughness pattern ( $\gamma = 1$ ). At the lower value of external load  $\bar{W}_0 = 2.5$ , the nonlinear analysis provides more value of critical journal mass for the stability of two lobe journal bearing ( $\delta = 1.20$ ,  $\delta = 1.0$ ) however, for the value of offset factor ( $\delta = 0.80$ ) linear analysis is more suitable for higher values of an external load ( $\bar{W}_0$ ) for isotropic roughness orientation pattern ( $\gamma = 1$ ). Further, to have more insight on the effect of roughness pattern on fluid film pressure distribution, the results of surface plots of pressure distribution are presented in Figure 7(a–h). For a chosen value of an external load  $\bar{W}_0 = 2.0$ , the value of maximum

fluid film pressure obtained by linear analysis is more for longitudinal and isotropic roughness pattern than that of a smooth and transverse roughness pattern. However, nonlinear analysis provides a larger value of fluid film pressure for transverse and isotropic pattern when compared with the smooth and transverse pattern for the same operating condition of bearing systems. This is because of resistance to the flow of the lubricant at the converging portion of bearing in case of isotropic pattern and transverse pattern. As a consequence of this, the lubricant gets accumulated at the converging portion which attributes to increase the fluid film pressure. The results presented in Figures 5 and 6, reveals that the stability parameter margin provided by the nonlinear analysis is higher for certain



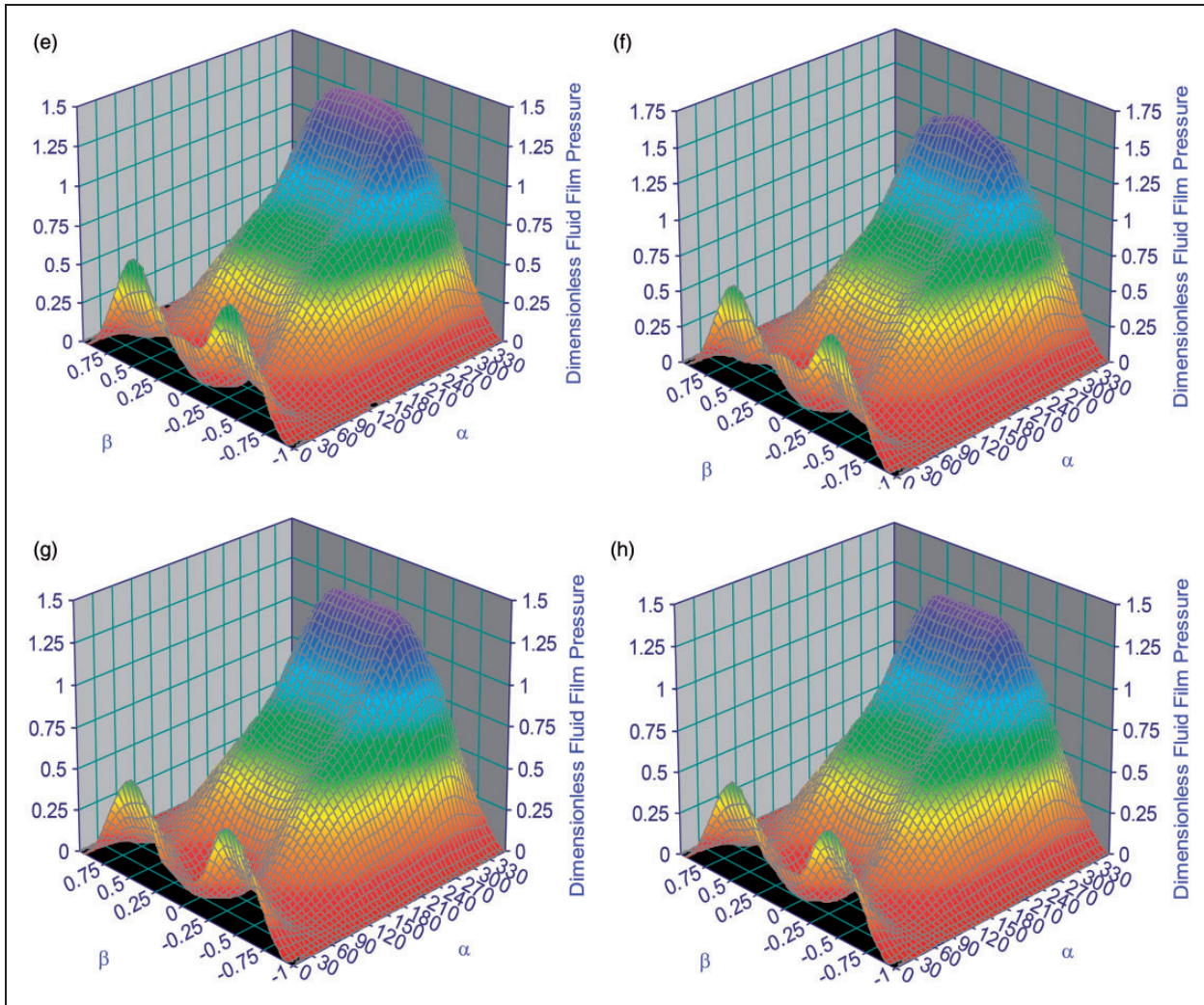
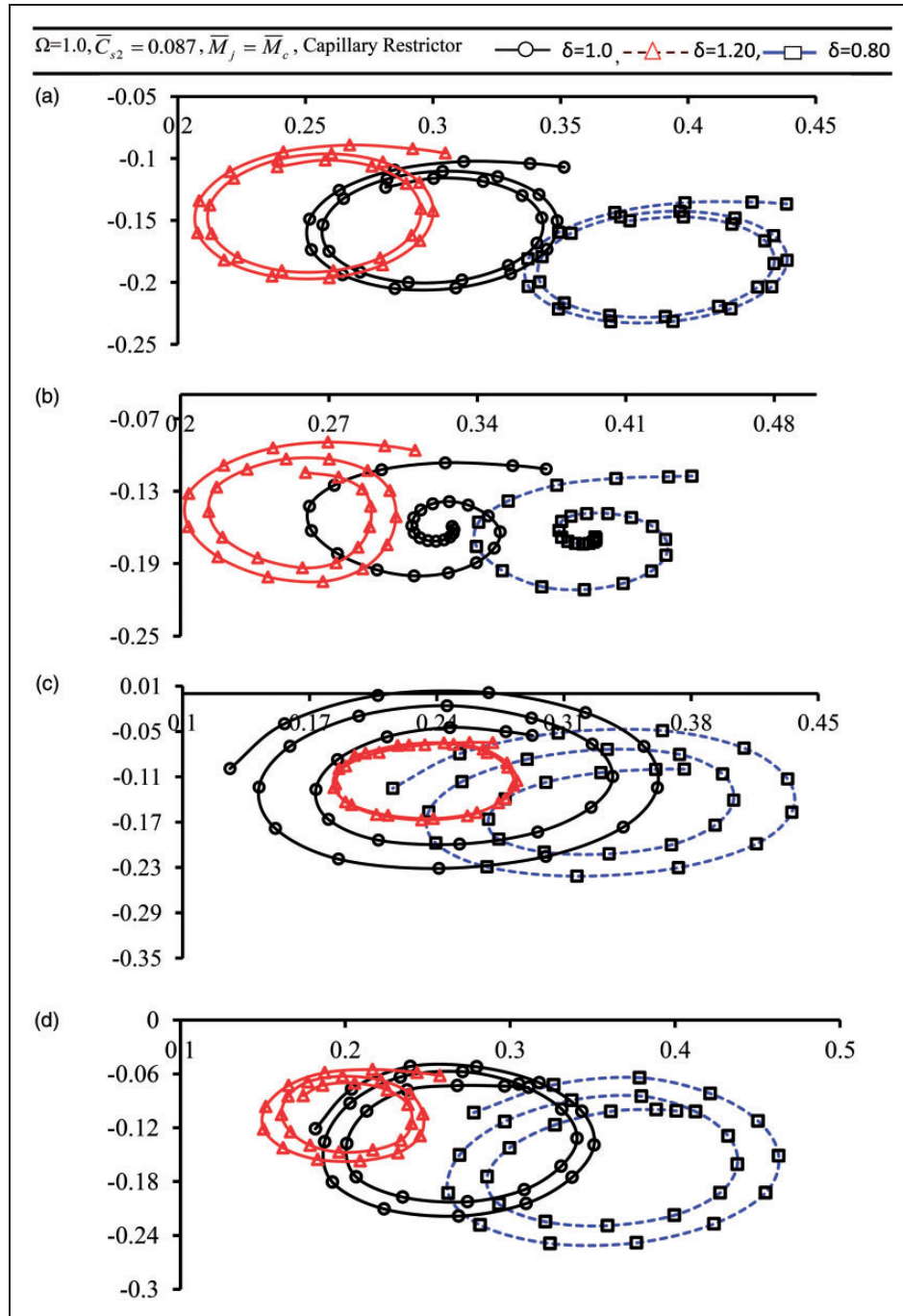


Figure 7. Continued.

values of an external load  $\bar{W}_0 \leq 3.0$  for the case of two lobe symmetric non recessed hybrid journal bearing at various roughness pattern parameter ( $\gamma$ ). Accordingly, the results are presented for various surface roughness pattern and different values of offset factor ( $\delta$ ) for three different cases when,  $\bar{M}_J = 1.1\bar{M}_c$ ,  $\bar{M}_J = \bar{M}_c$  and  $\bar{M}_J = 0.9\bar{M}_c$ . The non-linear journal center motion trajectories are presented in Figures 8–13 for 2-lobe hybrid journal bearing systems.

For  $\bar{M}_J = \bar{M}_c$  and  $\bar{W}_0 = 2.0$ , the influence of offset factor on the different roughness pattern parameter ( $\gamma$ ) have been presented in Figure 8(a–d) in terms of the non-linear journal motion trajectories for a 2-lobe symmetric hole entry hybrid journal bearing. From Figure 8(a) it may be noticed that when the journal mass equals the critical mass ( $\bar{M}_J = \bar{M}_c$ ) and smooth surface roughness pattern bearing is subjected to an external load of  $\bar{W}_0 = 2.0$ , then nonlinear equation of motion predicts a stable motion for all the values

of offset factor  $\delta = 0.80, 1.0$  and  $\delta = 1.20$ . Further, it may be observed that the bearing with the value of the offset factor  $\delta = 0.80$  traces a larger orbit for the same operating condition. Figure 8(b) indicates the locus of journal center motion for the transverse roughness pattern ( $\gamma = 1/6$ ). A non-linear equation of motion predicts a stable motion for  $\delta = 0.80$ ,  $\delta = 1.0$  and  $\delta = 1.20$  however, for the value of offset factor  $\delta = 0.80$  and  $\delta = 1.0$ , a locus of journal center approaches towards the center and settle down quickly. This is happening because of the transversely oriented asperities in a direction perpendicular to the direction of lubricant flow, which causes maximum resistance to the bearing flow in the direction of rotation thereby, increasing the side flow. But for the value of offset factor  $\delta = 1.20$ , the journal motion trajectories provide stable motion and operates at a minimum value of fluid film thickness at  $\gamma = 1/6$ . This is due to the change in bearing geometry.



**Figure 8.** (a–h) Trajectories for journal center motion for  $\bar{M}_j = \bar{M}_c$ .

Further, it restricts velocity-induced flow of the lubricant in the circumferential direction developing the converging section. As a result of this, the fluid-film pressure gets increased and hence the transverse roughness pattern ( $\gamma = 1/6$ ) gives higher film thickness. Figure 8(c) shows the non-linear journal motion for the longitudinal surface roughness pattern ( $\gamma = 6$ ) when the journal mass equals the critical mass

( $\bar{M}_j = \bar{M}_c$ ). It may be observed that journal motion trajectory provides unstable motion at an offset factor of  $\delta = 0.80, 1.0$  and traces a larger orbit. Further, at  $\delta = 1.20$  non-linear journal motion trajectory predicts limit cycle motion, in which; the locus of journal in the bearing neither converges nor diverges. When bearing with isotropic roughness pattern ( $\gamma = 1$ ) operates at external load of  $\bar{W}_0 = 2.0$  for

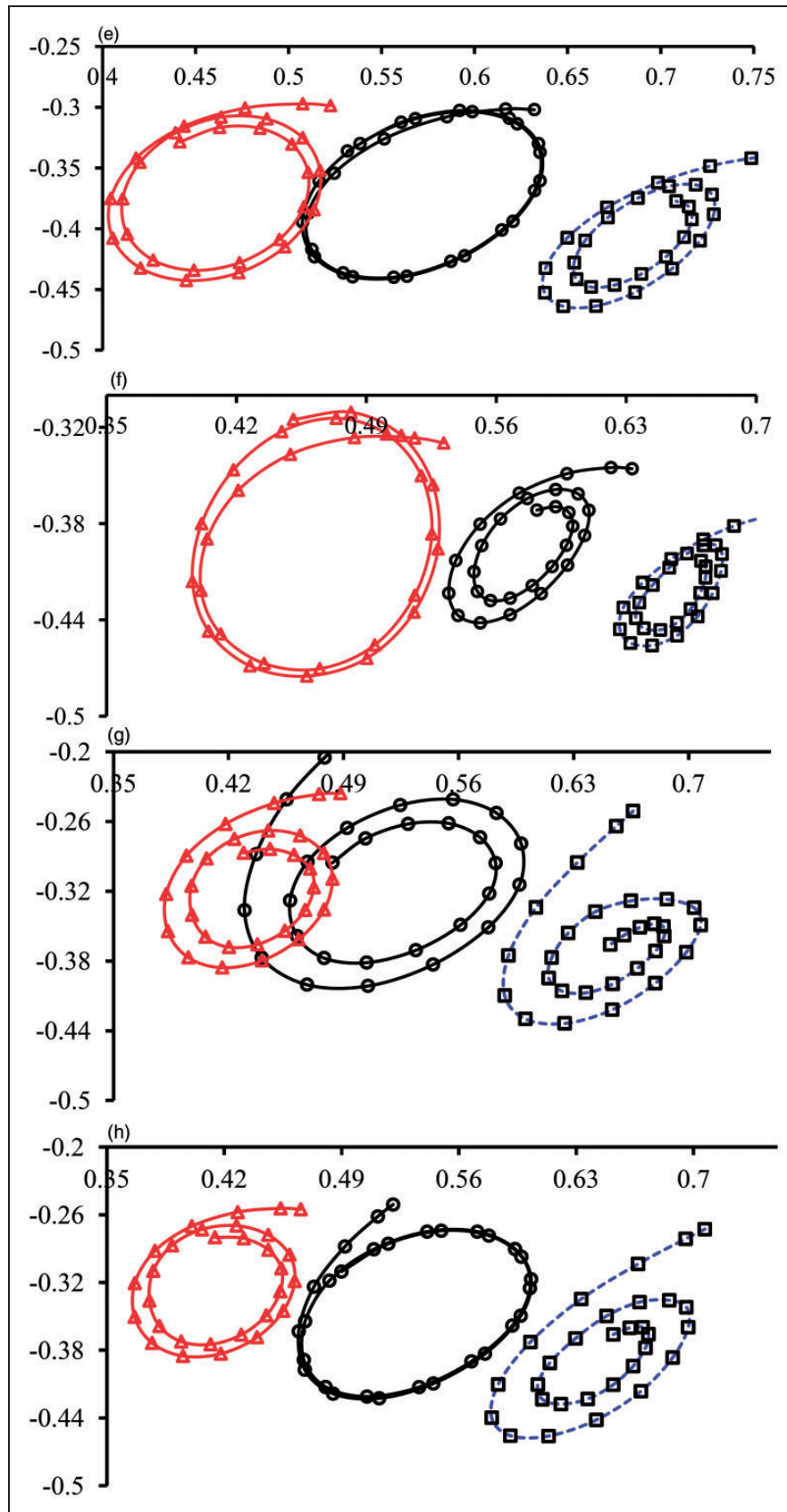
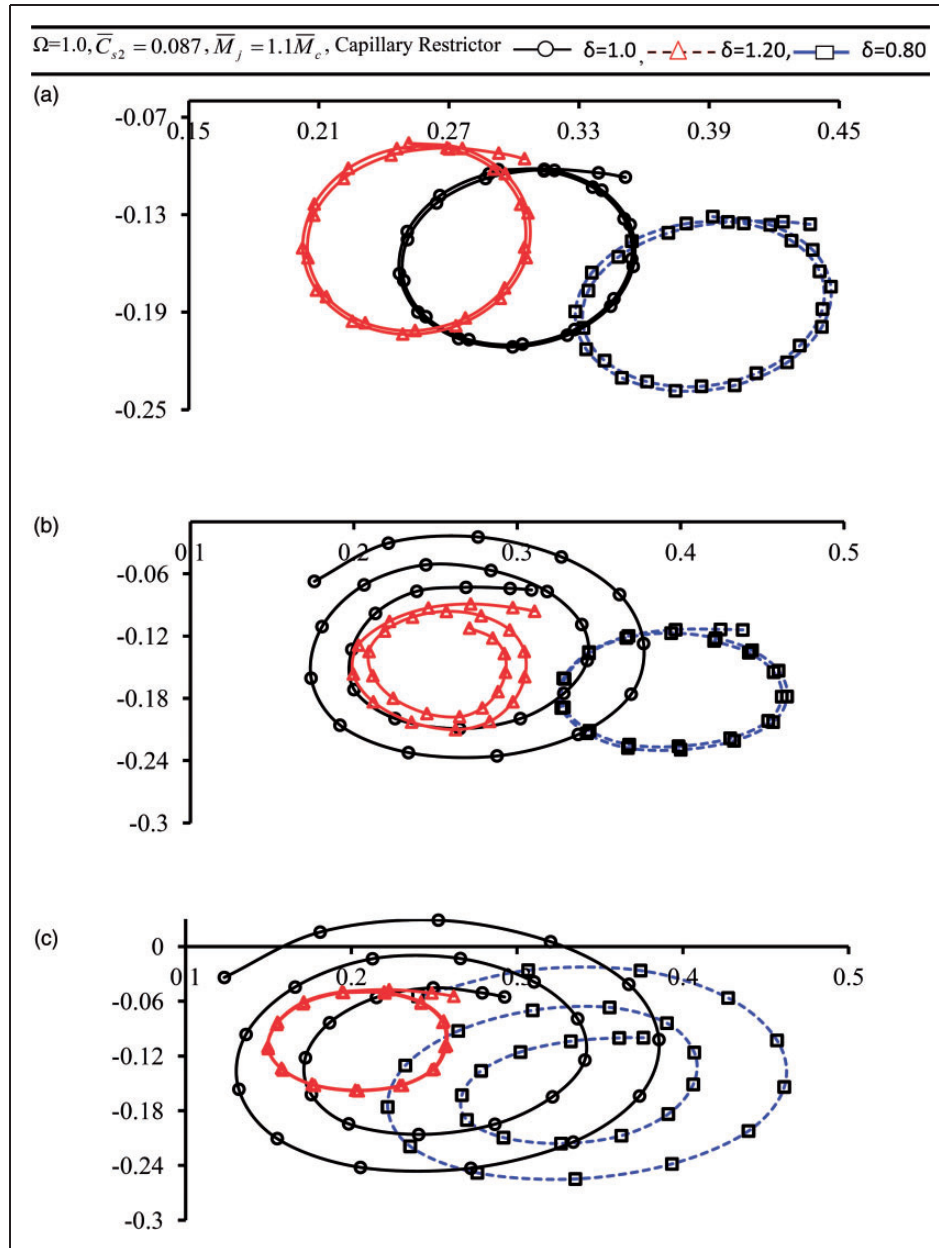


Figure 8. Continued.



**Figure 9.** (a–h). Trajectories for journal center motion for  $\bar{M}_J = 1.1\bar{M}_c$ .

the case of  $\bar{M}_J = \bar{M}_c$ . Then the non-linear journal motion trajectories provide unstable motion for two lobe bearing with offset factor  $\delta = 0.80$  and circular non-recessed hybrid journal bearing ( $\delta = 1.0$ ) as shown in Figure 8(d). Further it may be observed that the offset factor ( $\delta$ ) having value more than one predicts stable motion and traces small orbit, consequently, operates at lower value of minimum fluid film thickness. Therefore, from Figure 8(a–d), it may be stated that when the journal mass equals the critical mass, the non-linear transient journal motion predicts the stable motion for the value of

offset factor ( $\delta = 1.20$ ) for all the surface roughness pattern. Figure 8(e–h) show the non-linear journal motion trajectories when the journal mass is equal to the critical mass for two lobe non-recessed hybrid journal bearing at external load of  $\bar{W}_0 = 4.0$  for various roughness pattern.

Figure 8(e) shows the journal motion trajectories for smooth roughness pattern at  $\bar{W}_0 = 4.0$  for the different values of offset factor  $\delta = 0.8, 1.0$  and  $\delta = 1.20$ . a non-linear journal motion predicts stable motion for non-circular hybrid journal bearing ( $\delta = 0.8, 1.20$ ) and unstable motion for circular journal bearing ( $\delta = 1.0$ ).



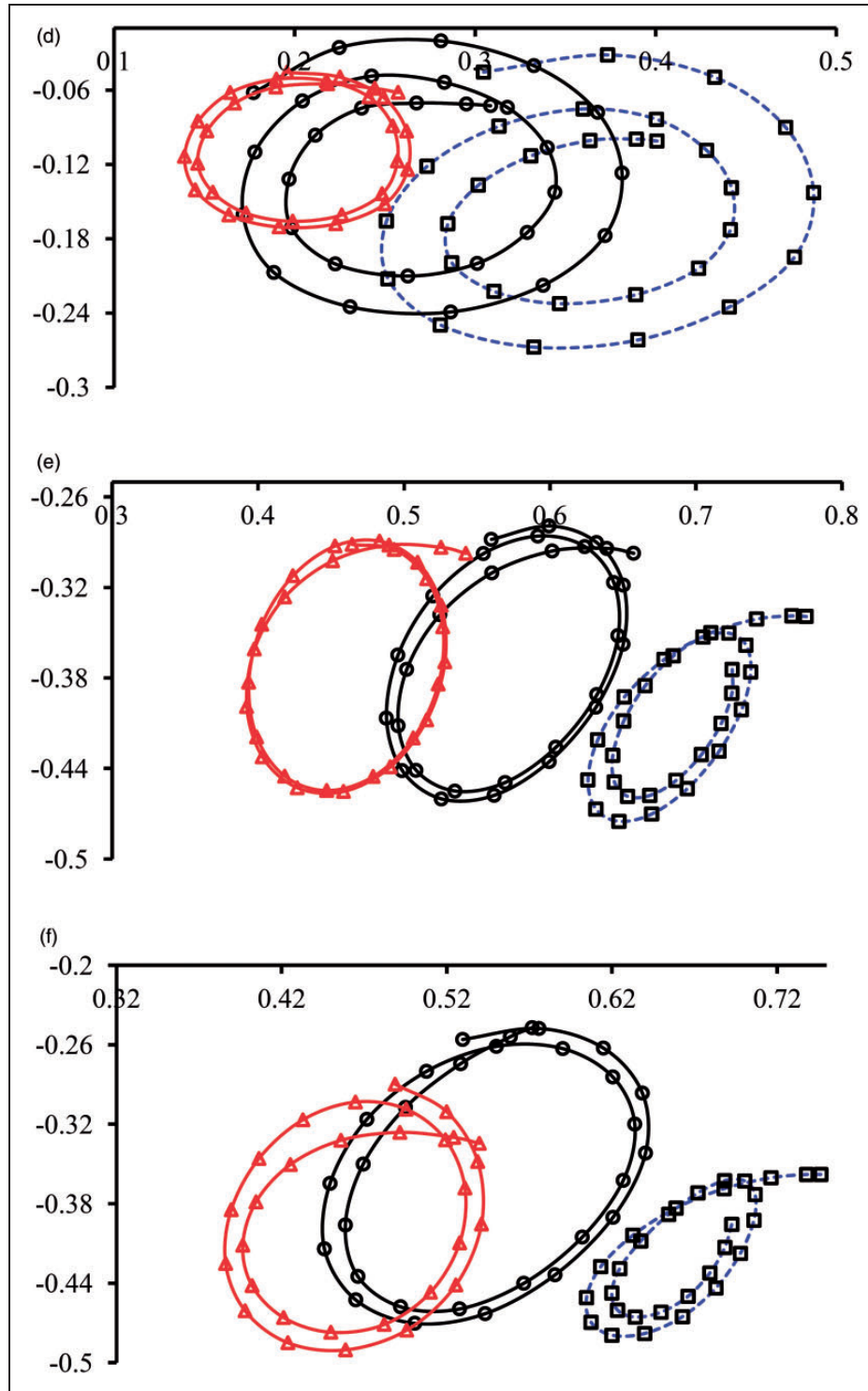


**Figure 9.** Continued.

For the value of external load  $\bar{W}_0 = 4.0$ , the transverse roughness pattern ( $\gamma = 1/6$ ), is having a noteworthy effect on bearing stability and the journal motion provides stable motion for circular bearing and forms limit cycle and unstable motion for non-circular journal

bearing. As shown in Figure 8(f), the bearing with offset factor,  $\delta = 1.1$  traces larger orbit. Therefore, there is a need to take care to prevent the bearing failure and to improve journal stability under the condition of bearing surface having the transverse roughness pattern



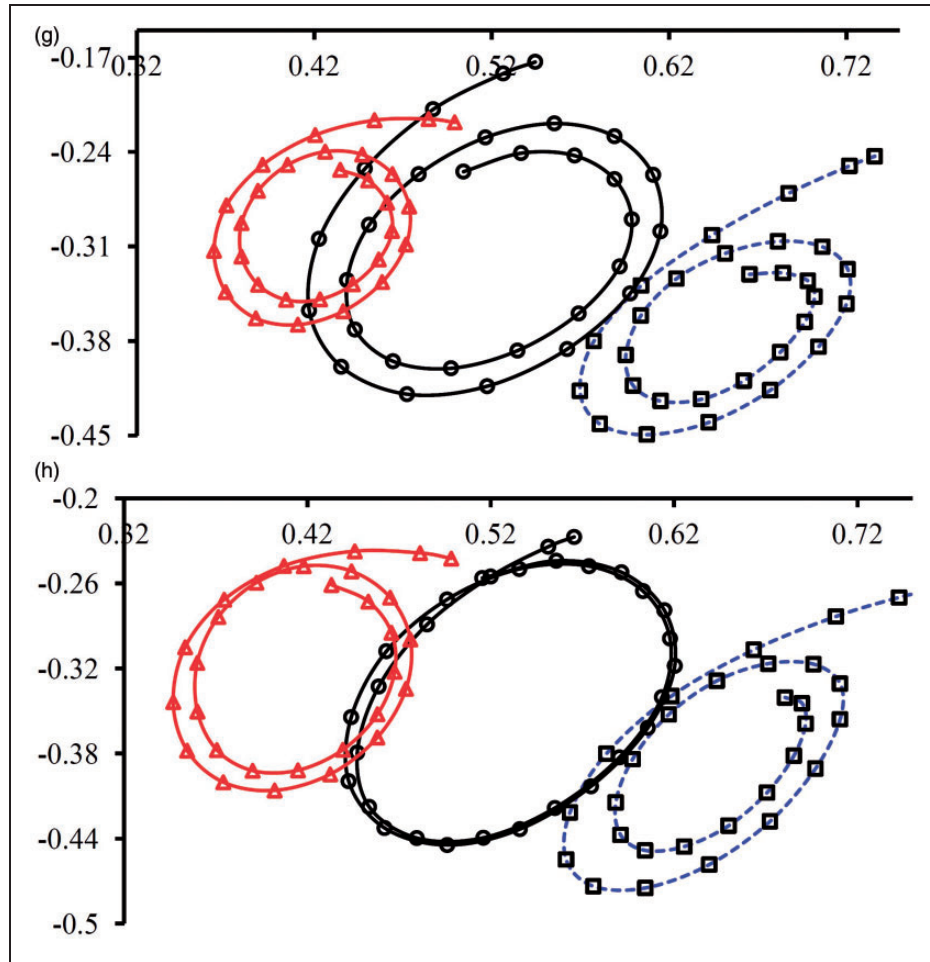


**Figure 9.** Continued.

( $\gamma = 1/6$ ). The journal motion trajectories for an external load  $\bar{W}_0 = 4.0$  and surface roughness pattern  $\gamma = 6$  is shown in Figure 8(g) when  $\bar{M}_J = \bar{M}_c$ . It may be seen from the Figure 8(g) that the journal motion trajectories predicts stable motion for all the value of offset factor ( $\delta$ ) considered in the study. As the load increases from  $\bar{W}_0 = 2.0$  to  $\bar{W}_0 = 4.0$ , the nonlinear transient analysis shows stable motion, whereas; at  $\bar{W}_0 = 2.0$  for the same operating parameters (Figure 8(c)), journal motion trajectories report unstable motion. This is because of more velocity-induced flow of the lubricant in circumferential direction. Further, an increase in the value load ( $\bar{W}_0$ ) increases the bearing eccentricity and journal moves towards the downward direction forming converging section, as a result of this, the bearing is supplied with more lubricant to bear the applied load. Figure 8(h) shows the non-linear journal motion trajectories for isotropic roughness pattern ( $\gamma = 1$ ). For the value of the offset factor  $\delta = 1.2$  and  $\delta = 0.8$ , the journal motion provides stable motion, whereas for the value of  $\delta = 1.0$ , journal motion predicts the limit

cycle motion. That means the non-circular journal bearing provides stable motion because of maximum clearance and it is greater than the circular journal bearing. Owing to this, the fluid film pressure is concentrated in the narrow region of the bearing gap. This would help to balance the hydrodynamic oil film force component and applied load. As a consequence of this, it shows the less effect of disturbance.

Figure 9 (a–d) depicts the nonlinear journal trajectory motion plots for  $\bar{M}_J = 1.1\bar{M}_c$  and  $\bar{W}_0 = 2.0$ . Figure 9(a) indicates the journal center motion orbit, when journal and bearing surfaces are smooth. The journal motion predicts unstable motion for all the values of offset factor ( $\delta$ ). But when the roughness pattern changes from smooth surface to transverse pattern ( $\gamma = 1/6$ ), the nonlinear equation of motion traces an unstable motion for circular bearing ( $\delta = 1.0$ ) and limit cycle motion for the value of offset factor  $\delta = 0.80$ . Further from Figure 9(b), it may be observed that for the value of offset factor more than one, i.e.  $\delta = 1.20$ , the journal center motion provides stable motion. This

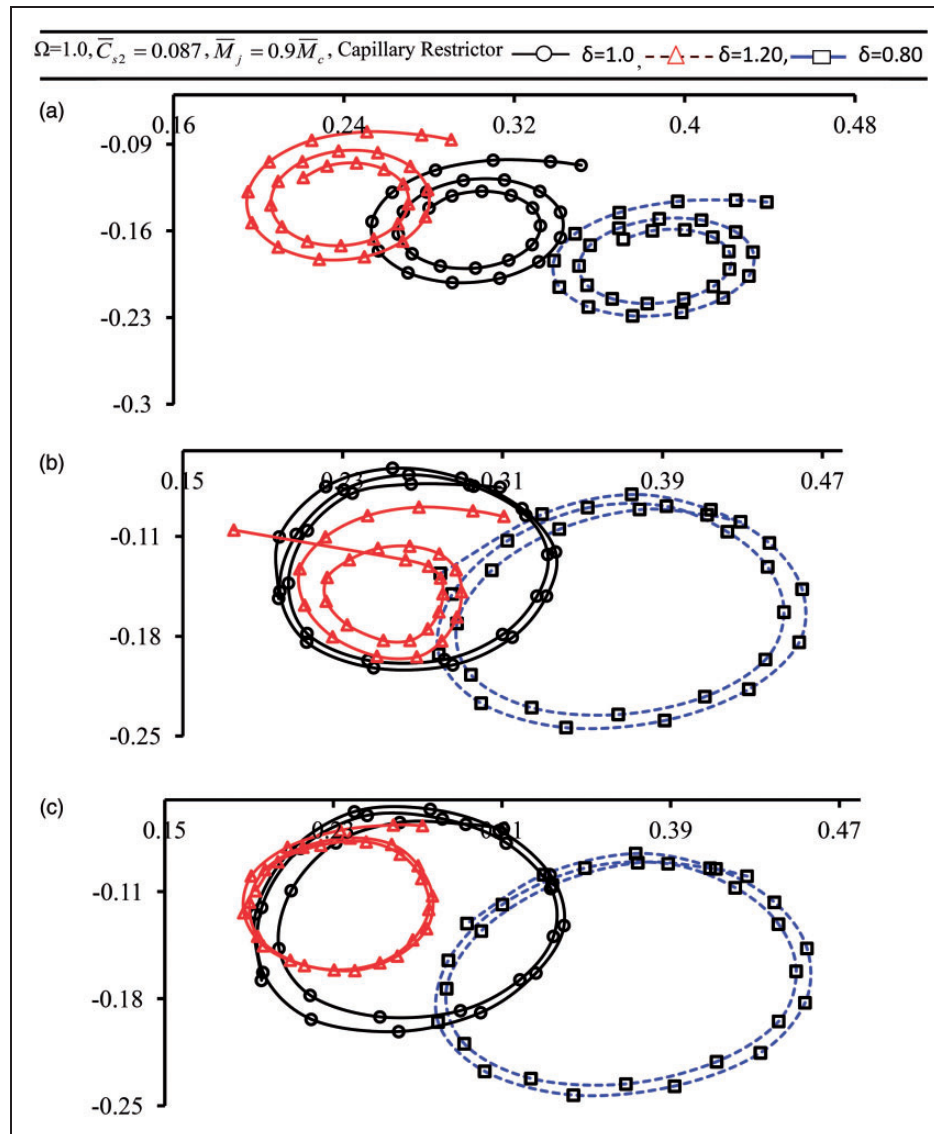


**Figure 10.** (a–h). Trajectories for journal center motion for  $\bar{M}_j = 0.9\bar{M}_c$ .

happens due to the change of bearing geometry, which increases the eccentricity of the bearing system. The nonlinear journal motion trajectories for longitudinal roughness pattern ( $\gamma = 6$ ) and isotropic roughness pattern ( $\gamma = 1$ ) when  $\bar{M}_j = 1.1\bar{M}_c$  are shown in Figure 9(c–d). For the value of offset factor  $\delta = 0.80, 1.0$ , the journal motion traces unstable orbit while for the value of  $\delta = 1.20$ , it traces limit cycle motion. These results are anticipated because of the journal mass is greater than the critical mass.

The journal motion trajectories for the value of an external load  $\bar{W}_0 = 4.0$  when  $\bar{M}_j = 1.1\bar{M}_c$ , is presented in Figure 9(e–h) for all the values of offset factor. Figure 9(e) depicts the nonlinear equation of journal

center motion trajectories for smooth surface bearing. The journal motion traces limit cycle motion for circular ( $\delta = 1.0$ ) and noncircular bearing geometries ( $\delta = 0.80, 1.2$ ). When  $\bar{M}_j = 1.1\bar{M}_c$ , at  $\bar{W}_0 = 4.0$  and  $\gamma = 1/6$ , the nonlinear journal center motion predicts limit cycle motion which is indicated in Figure 9(f). This is due to transverse roughness pattern ( $\gamma = 1/6$ ) which provides axial flow and restricts the flow of lubricant in circumferential direction. As a consequence of this, at higher values of external load, the bearing operates at lower quantities of lubricant flow.

From Figure 9(g–h) it may be noticed that when the surface roughness becomes longitudinal ( $\gamma = 6$ ) and isotropic ( $\gamma = 1$ ), the nonlinear equation of journal

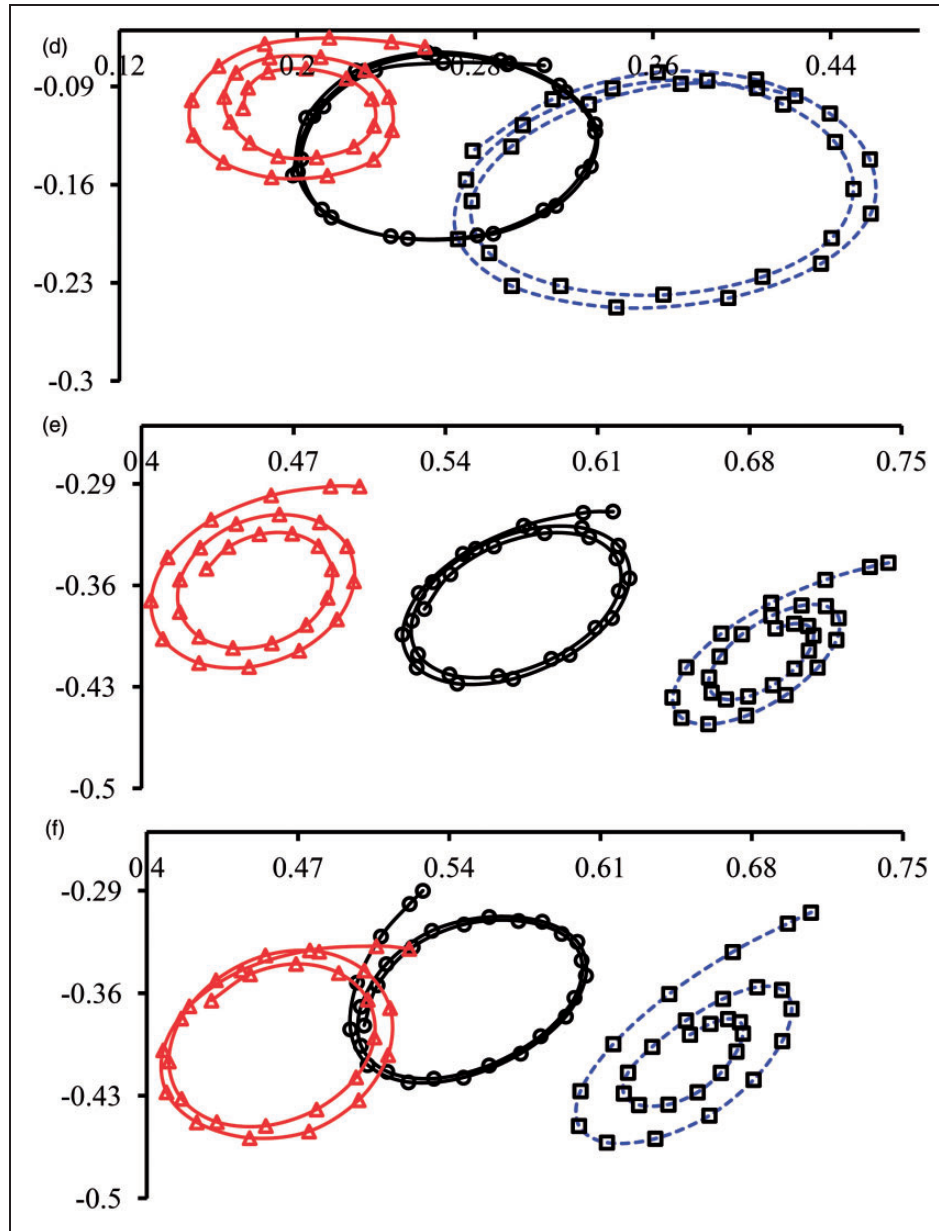


**Figure 10.** Continued.

motion predicts stable motion even though the  $\bar{M}_j = 1.1\bar{M}_c$  for non circular journal bearing ( $\delta \geq 1.0$ ). These surface roughness patterns provide a large quantity of lubricant flow in the circumferential direction and support the load acting on it. As a result of this, journal motion predicts stable motion. But for isotropic pattern ( $\gamma = 1$ ) circular journal bearing ( $\delta = 1.0$ ) provides the limit cycle motion. A notable observation that can be revealed from the journal orbit is that the journal motion forms a stable motion cycle for noncircular journal bearing ( $\delta = 1.20$  and  $\delta = 0.80$ ) on the higher operational value of an external load  $\bar{W}_0 = 4.0$  when  $\bar{M}_j = 1.1\bar{M}_c$ . Further for the lower values of  $\bar{W}_0 = 2.0$ ,

nonlinear equation of motion provides stable motion when the offset factor is greater than one ( $\delta = 1.20$ ).

The nonlinear journal motion trajectories for  $\bar{M}_j = 0.9\bar{M}_c$  is shown in Figure 10(a–h). Figure 10(a–d) depicts the nonlinear journal motion trajectories for the value of an external load  $\bar{W}_0 = 2.0$ . When the bearing and journal surface is smooth, the nonlinear trajectory form stable motion. Obviously, these results are anticipated as the journal mass is less than the critical mass and a journal motion form stable motion for all the values of offset factor. Figure 10(b) depicts the journal motion orbit for the value of  $\gamma = 1/6$  and  $\bar{W}_0 = 2.0$ . When the journal and

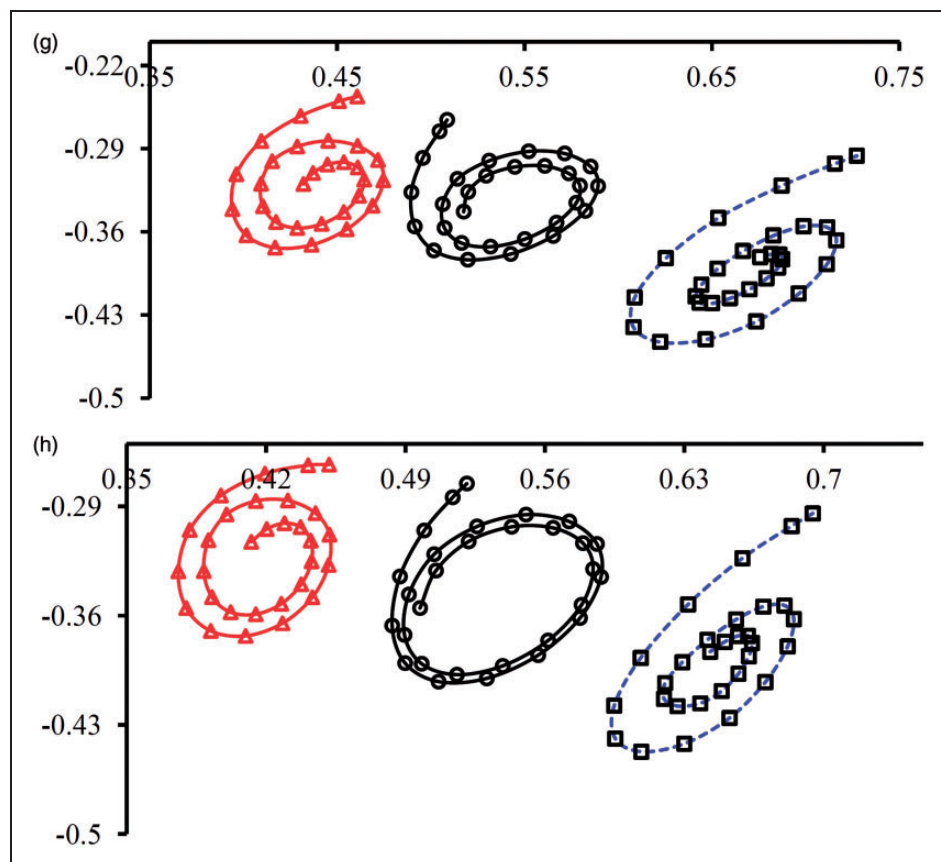


Figure 10. Continued.

bearing surface are having a transverse roughness pattern ( $\gamma = 1/6$ ), the bearing with offset factor  $\delta = 1.20$ , predict stable motion, whereas, for the value of  $\delta = 1.0$  and  $\delta = 0.8$ , it predicts unstable motion. As shown in Figure 10(c), as the rough surface orientation becomes longitudinal ( $\gamma = 6$ ), the nonlinear equation of motion provides unstable and limit cycle motion for the values of  $\delta = 0.8, 1.0$  and  $\delta = 1.20$  respectively. The journal motion trajectories for the isotropic roughness pattern ( $\gamma = 1$ ) are shown in Figure 10(d). For isotropic roughness pattern ( $\gamma = 1$ ), at the value of  $\delta = 1.20$ , the journal motion predicts stable motion, whereas the circular bearing ( $\delta = 1.0$ ) forms limit cycle motion. In general, it may be concluded that for the lower value of an external load  $\bar{W}_0 = 2.0$  and  $\bar{M}_f = 0.9\bar{M}_c$ , the transverse ( $\gamma = 1/6$ ) and isotropic roughness ( $\gamma = 1$ ) pattern provides stable motion with smaller size of the motion orbit at the value of  $\delta = 1.20$ . Further, it may be noticed that the size of the journal motion orbit becomes larger for the values of  $\gamma = 1/6$ ,  $\gamma = 1$  and  $\gamma = 6$  and bearing operates at large eccentricity ratio at  $\delta = 0.8$ .

The journal motion trajectories for the value of an external load  $\bar{W}_0 = 4.0$  are presented in Figure 10(e–h). For all the roughness pattern parameter, including

smooth surface, the nonlinear equation of motion predicts stable motion for all the values of offset factor. The longitudinal roughness pattern orientation ( $\gamma = 6$ ) provides stable motion with smaller orbit size for the value of  $\delta = 1.20$  and  $\delta = 1.0$ . This is because of the orientation of roughness pattern. The bearing with offset factor  $\delta = 0.8$  form stable motion with the larger size of the journal motion orbit (Figure 10(f–h)) and operates at larger values of eccentricity ratio and minimum value of fluid film thickness. Therefore, even though the stable motion predicted at the value of  $\delta = 0.8$  for all surface roughness pattern, the designer may take proper care while choosing an appropriate roughness pattern to obtain an improved value of stability.

Figures 11–13 depicts the influence of roughness pattern parameter ( $\gamma$ ) on the journal center motion trajectory for different values of offset factor ( $\delta$ ) and an external load. Figure 11(a–c) indicates the nonlinear journal center motion orbits when  $\bar{M}_f = \bar{M}_c$  at  $\bar{W}_0 = 2.0$ . As indicated in Figure 11(a), for the value of  $\delta = 0.8$ , the journal center motion exhibit the stable motion for transverse pattern ( $\gamma = 1/6$ ) while form limit cycle motion for smooth pattern bearing. Further it may be noticed that, the nonlinear equation

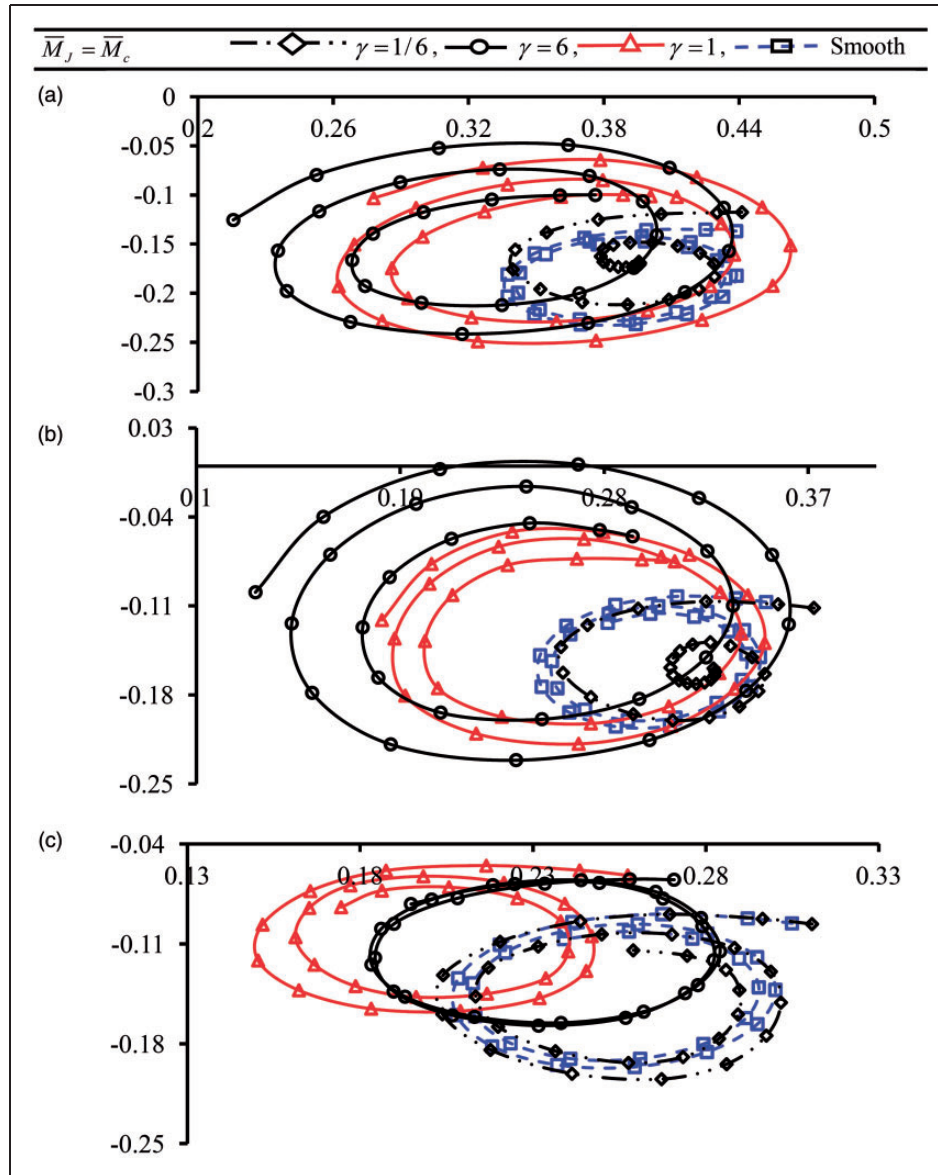


**Figure 11.** (a–f). Trajectories for journal center motion for various offset factor ( $\delta$ ) and  $\bar{M}_j = \bar{M}_c$ .

of motion provides unstable motion for longitudinal ( $\gamma = 6$ ) and isotropic roughness pattern ( $\gamma = 1$ ). This happens because of change in bearing geometry. Moreover, the same trend of stability of journal motion is observed in Figure 11(b) when the circular bearing ( $\delta = 1.0$ ) operates at external load of  $\bar{W}_0 = 2.0$  for the entire roughness pattern. When the non circularity of the two lobe hole entry hybrid journal bearing is increased to offset factor  $\delta = 1.20$ , the journal motion forms stable cycle motion for  $\gamma = 1/6$ ,  $\gamma = 1$  and smooth surface. For longitudinal roughness pattern ( $\gamma = 6$ ), nonlinear equation of motion predicts limit cycle motion when  $\bar{M}_j = \bar{M}_c$ . Additionally, it may be observed that when the bearing operates at lower value of external load  $\bar{W}_0 = 2.0$  and offset factor  $\delta = 0.8$ , the

transverse roughness pattern ( $\gamma = 1/6$ ) provides stable motion with smaller journal motion orbit than the longitudinal ( $\gamma = 6$ ) and isotropic roughness pattern ( $\gamma = 1$ ). The nonlinear journal motion trajectory at higher values of external load  $\bar{W}_0 = 4.0$  for  $\bar{M}_j = \bar{M}_c$  is shown in Figure 11(d–f). Figure 11(d) indicates the journal center motion at  $\delta = 0.8$  when  $\bar{M}_j = \bar{M}_c$ . The journal center motion provides stable motion for longitudinal ( $\gamma = 6$ ), smooth and isotropic roughness pattern ( $\gamma = 1$ ) whereas, forms limit cycle motion for the transverse roughness pattern ( $\gamma = 1/6$ ). That means longitudinal, smooth and isotropic roughness pattern has more influence on stability at higher values of external load. The circular hole entry hybrid journal bearing compensated with capillary restrictor



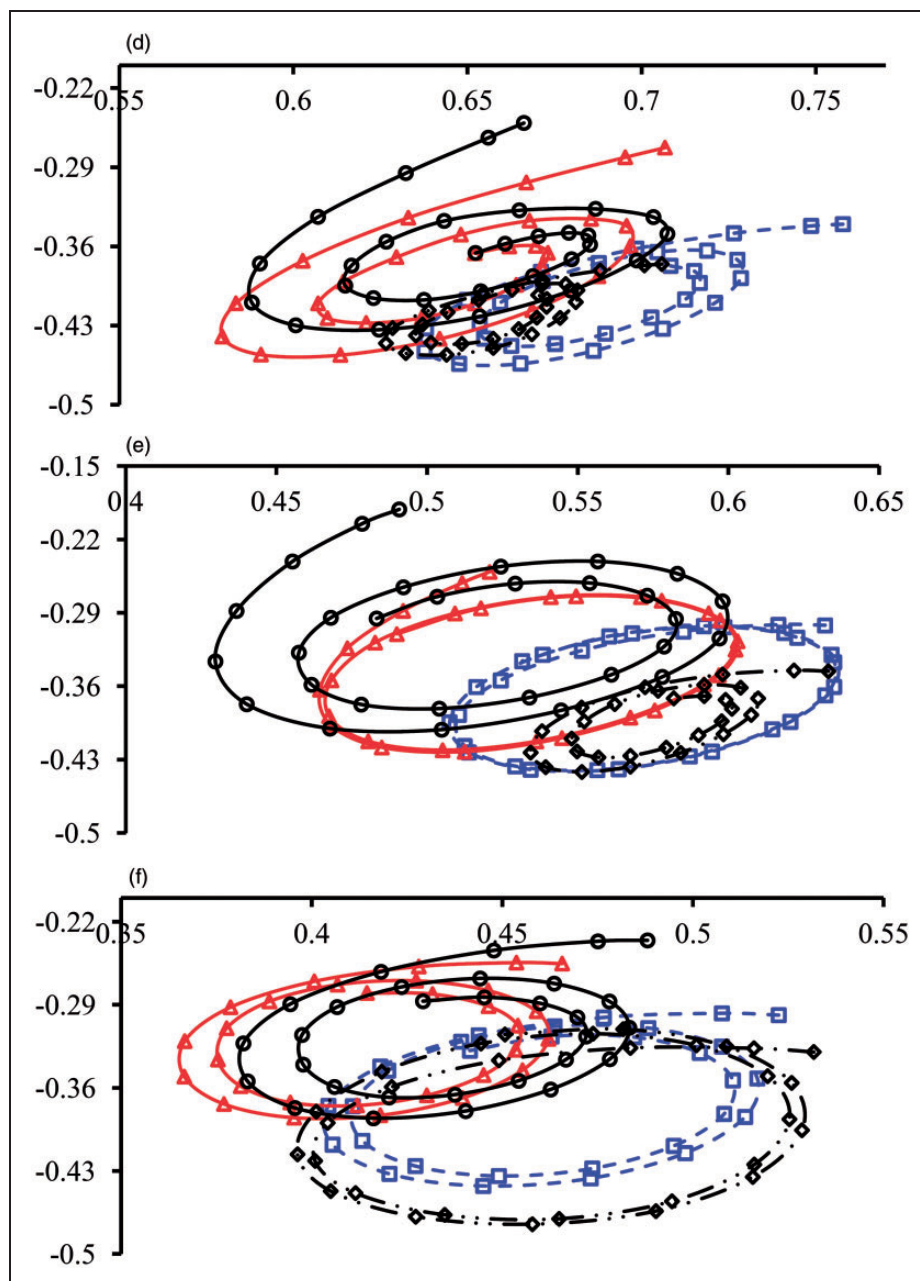
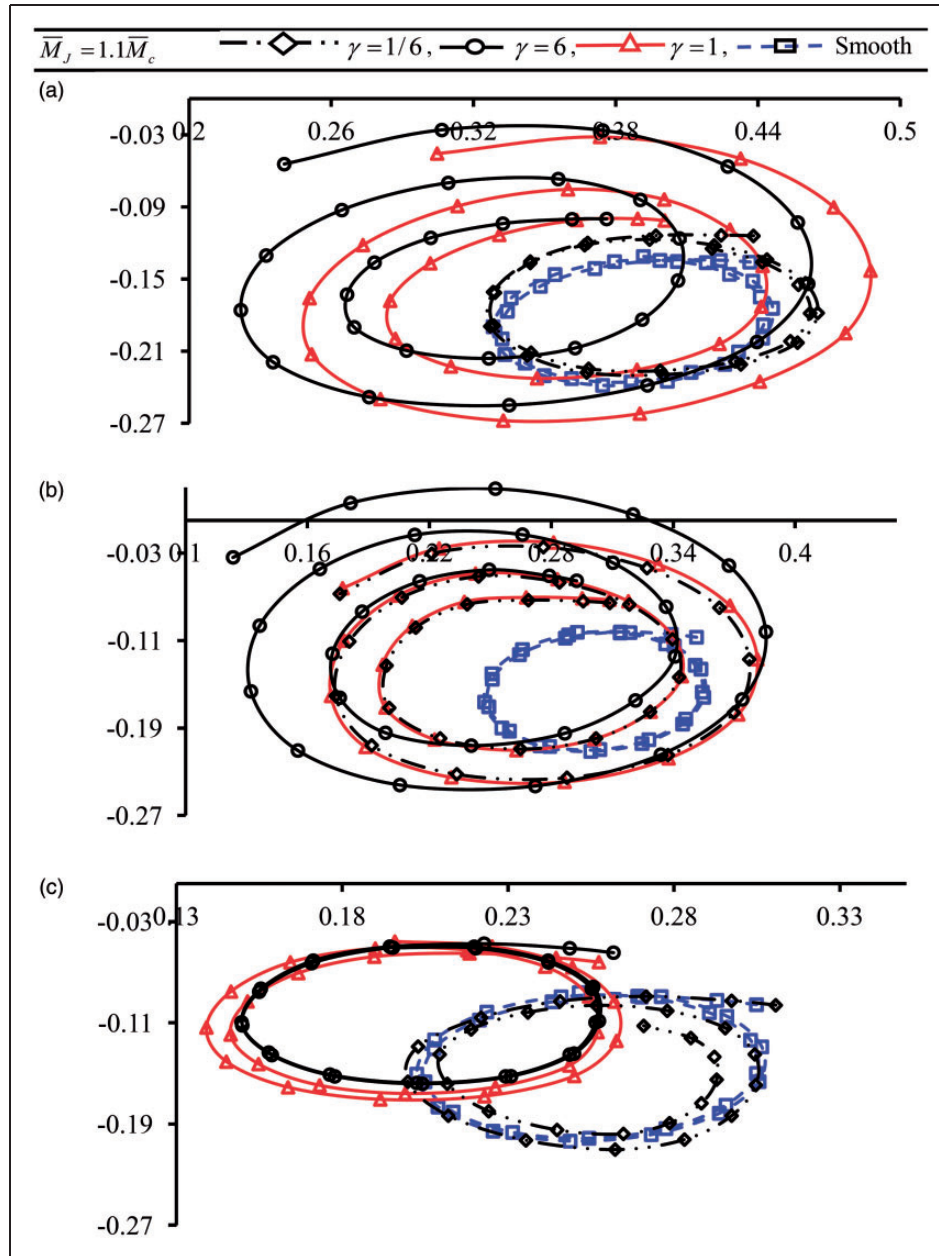


Figure 11. Continued.

exhibits the stable journal motion for all the roughness pattern except the smooth surface. From Figure 11(e), it may be observed that, when  $\gamma = 6$ , the journal operates at lower values of the eccentricity ratio than the smooth and transverse roughness pattern ( $\gamma = 1/6$ ) bearing. The nonlinear journal center motion trajectory for the value of offset factor  $\delta = 1.20$  is shown in Figure 11(f). Due to change in bearing geometry and increase in the value of an external load, the journal motion orbit provides stable motion for the entire roughness

pattern when  $\bar{M}_j = \bar{M}_c$ . This is an important result from the stability point of view; to be considered in favor of all roughness patterns and the non circular journal bearing. The journal motion trajectories for  $\bar{M}_j = 1.1\bar{M}_c$  and  $\bar{W}_0 = 2.0$  is shown in Figure 12(a–c). Figure 12(a) depicts the journal motion trajectory at  $\delta = 0.80$ . The trajectory forms unstable motion cycle for longitudinal ( $\gamma = 6$ ) and isotropic roughness pattern ( $\gamma = 1$ ) and limit cycle motion for transverse and smooth pattern. As shown in Figure 12(b), the



**Figure 12.** (a–f). Trajectories for journal center motion for various offset factor ( $\delta$ ) and  $\bar{M}_j = 1.1\bar{M}_c$ .

nonlinear equation of journal motion predicts unstable motion for all the roughness pattern except the smooth surface. The smooth surface pattern exhibits limit cycle motion when  $\bar{M}_j = 1.1\bar{M}_c$ . As the bearing becomes noncircular with the value of offset factor  $\delta = 1.20$ , the transverse roughness pattern ( $\gamma = 1/6$ ) provides stable motion and other pattern ( $\gamma = 6, 1$ ) including smooth surface form limit cycle motion. Further from Figure 12(c), it may be observed that the bearing with transverse roughness pattern ( $\gamma = 1/6$ ) operates at

lower values of minimum fluid film thickness when  $\bar{M}_j = 1.1\bar{M}_c$ . These are interesting results concerning the stability. Figure 12(d–g) shows the influence of the roughness pattern on journal center motion trajectory at  $W_0 = 4.0$  and  $\bar{M}_j = 1.1\bar{M}_c$ . Figure 12(d) depicts the journal motion trajectory for the value of offset factor  $\delta = 0.80$ . The longitudinal ( $\gamma = 6$ ) and isotropic rough surface ( $\gamma = 1$ ) bearing trace the stable motion orbit while smooth and transverse ( $\gamma = 1/6$ ) surface bearing predicts unstable motion. As indicated in Figure 12(e),

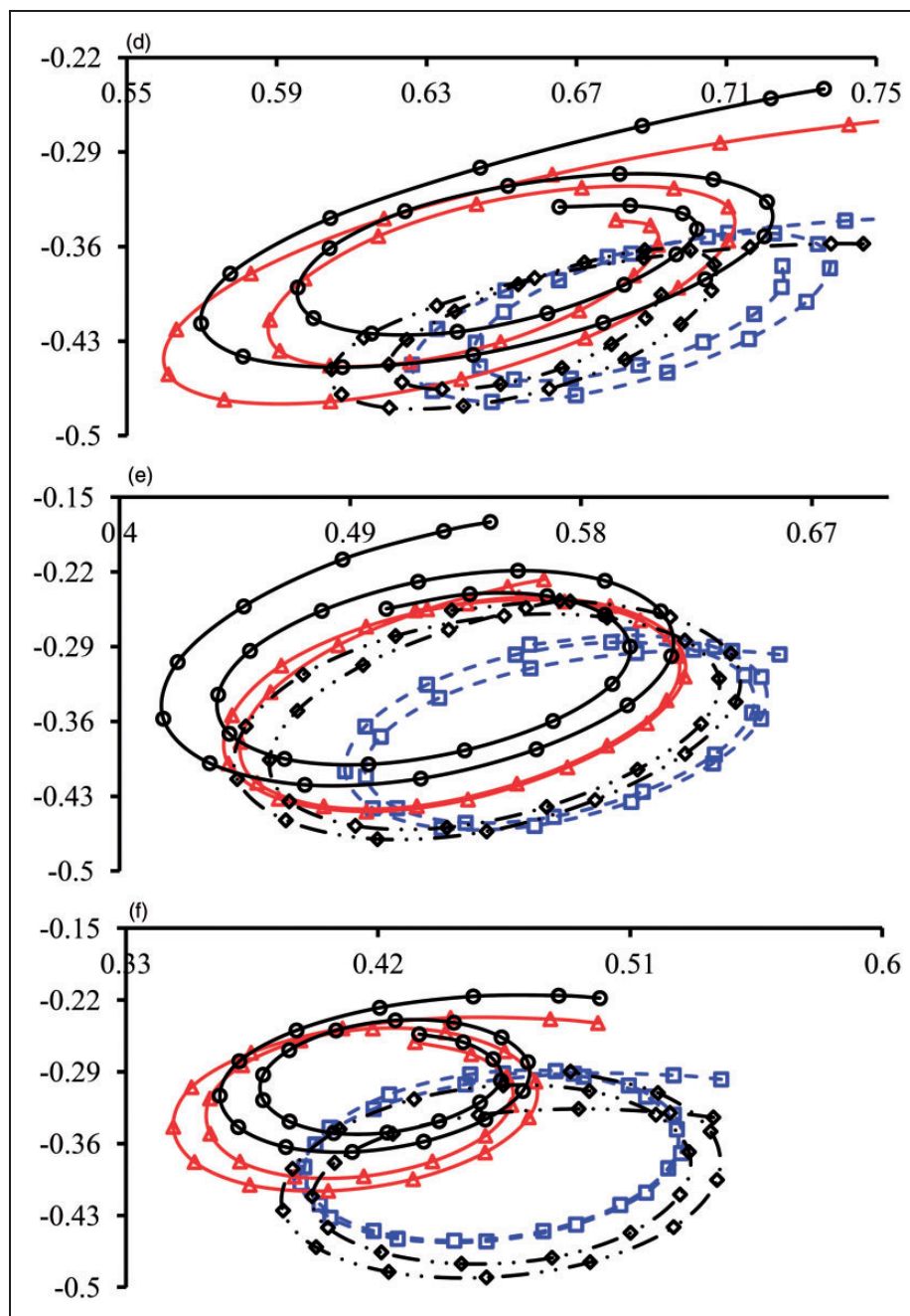
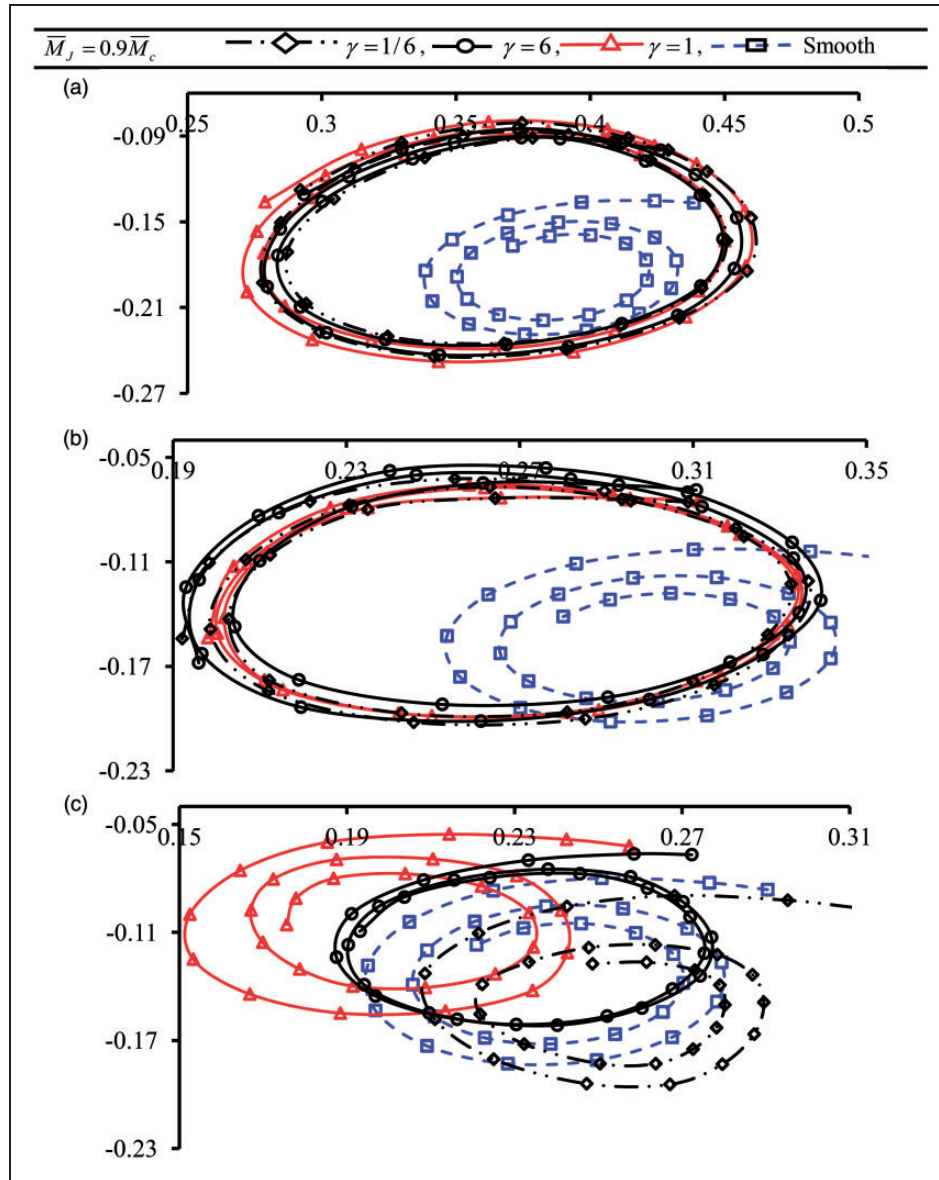


Figure 12. Continued.

it may be revealed that as the bearing operates at larger values of external load  $\bar{W}_0 = 4.0$ , the nonlinear equation of journal center motion traces a stable trajectory for longitudinal roughness pattern ( $\gamma = 6$ ) and form limit cycle motion for isotropic pattern ( $\gamma = 1$ ). The smooth and transverse pattern provides the unstable motion for the value of offset factor  $\delta = 1.0$ . When offset factor  $\delta = 1.20$  and  $\bar{M}_j = 1.1\bar{M}_c$ ; the journal center motion equation predicts stable motion for isotropic ( $\gamma = 1$ ) and longitudinal pattern ( $\gamma = 6$ ) whereas;

the smooth and transverse pattern ( $\gamma = 1/6$ ) traces the unstable motion trajectory which diverges towards the outside and makes the system unstable. From Figure 12(a-f), the noteworthy observation may be revealed that when bearing roughness pattern is isotropic ( $\gamma = 1$ ) and longitudinal ( $\gamma = 6$ ), journal motion predicts stable motion for an offset factor greater than one when the journal mass is greater than the critical mass for the value of an external load  $\bar{W}_0 = 4.0$  and traces stable cycle for transverse roughness pattern when



**Figure 13.** (a–f) Trajectories for journal center motion for various offset factor ( $\delta$ ) and  $\bar{M}_j = 0.9\bar{M}_c$ .

$\bar{W}_0 = 2.0$ . The nonlinear motion trajectories for  $\bar{W}_0 = 2.0$  and  $\bar{M}_j = 0.9\bar{M}_c$  are shown in Fig. 13 (a–c). As shown in Figure 13(a), when offset factor  $\delta = 0.8$ , the nonlinear journal center motion trajectories yields stable motion for smooth surface bearing whereas, predicts unstable motion for transverse ( $\gamma = 1/6$ ), isotropic ( $\gamma = 1$ ) and longitudinal roughness pattern ( $\gamma = 6$ ). The smooth surface bearing exhibits stable motion when bearing operates at the value of an external load  $\bar{W}_0 = 2.0$  and  $\delta = 1.0$ . Further, from Figure 13(b), it may be noticed that the nonlinear equation of journal center motion predicts the limit cycle motion for transverse and the isotropic roughness pattern ( $\gamma = 1$ ) and the unstable motion for longitudinal

pattern ( $\gamma = 6$ ). As the value of bearing non circularity defined by the offset factor is increased to  $\delta = 1.20$ , the journal center motion yields stable motion for all the values of roughness pattern. The bearing with smooth surface pattern and transverse pattern ( $\gamma = 1/6$ ) runs at higher eccentricity ratio and operates at a lower value of minimum fluid film thickness. Therefore, it may be concluded that when the journal mass is less than the critical mass ( $\bar{M}_j = 0.9\bar{M}_c$ ), the nonlinear equation of journal center motion predicts unstable motion for transverse ( $\gamma = 1/6$ ), the isotropic and longitudinal roughness orientation ( $\gamma = 6$ ) for the value of  $\delta = 1.0$  and  $\delta = 0.8$  except the smooth surface. The nonlinear journal center motion trajectories for  $\bar{W}_0 = 4.0$  and



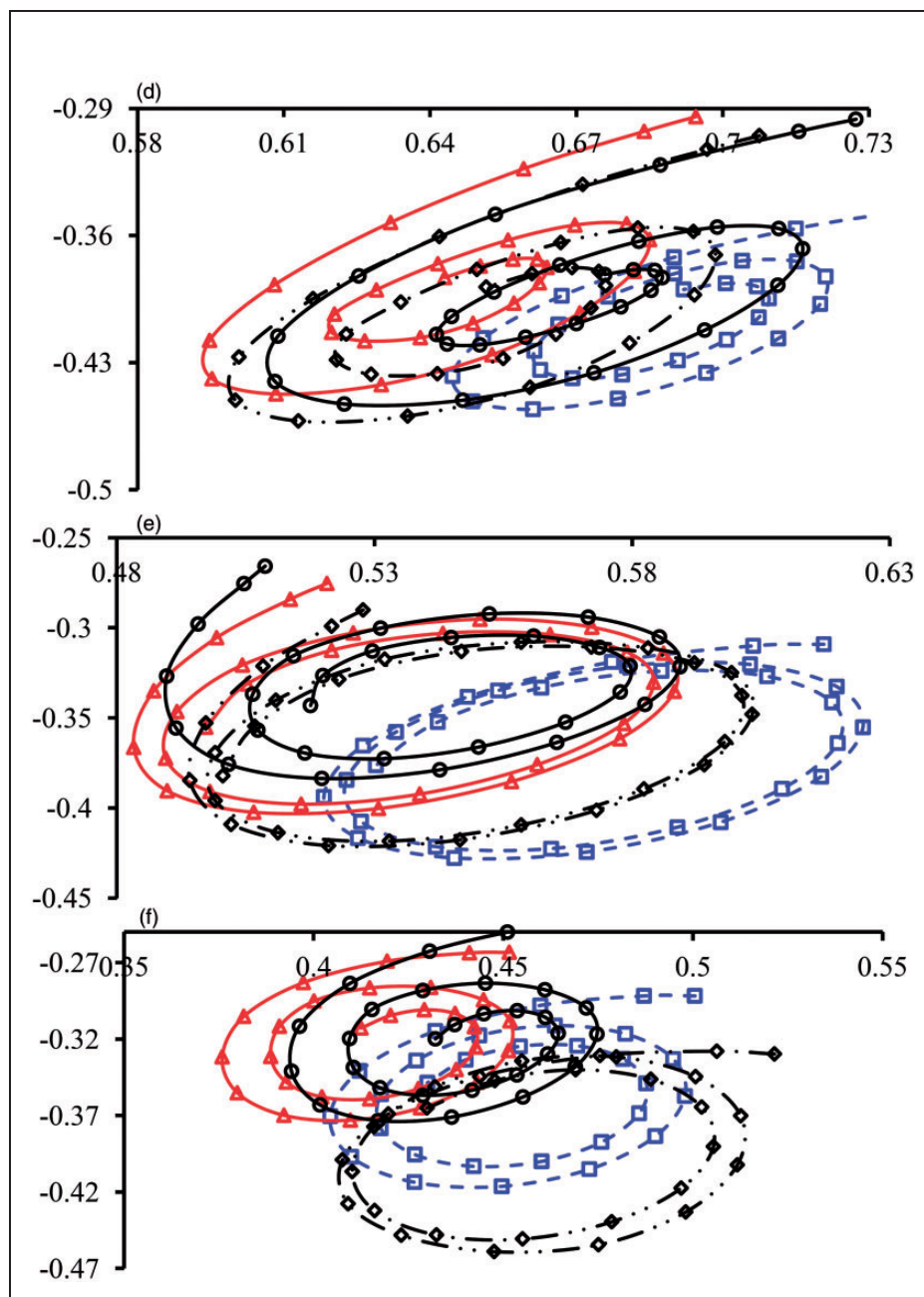


Figure 13. Continued.

$\bar{M}_j = 0.9\bar{M}_c$  are shown in Figure 13(d-f). The nonlinear trajectories form stable motion cycle for all the values of roughness pattern. (smooth,  $\gamma = 1/6$ ,  $\gamma = 1$ ,  $\gamma = 6$ ) at all the values of offset factor ( $\delta = 1.20, 1.0, 0.80$ ).

It may be observed that the surface roughness pattern has more influence on stability at lower values of external load ( $\bar{W}_0 = 2.0$ ) and provides stable motion at higher values of external load ( $\bar{W}_0 = 4.0$ ) when  $\bar{M}_j = 0.9\bar{M}_c$ . Therefore, for a symmetric non recessed journal bearing system compensated with capillary restrictor, bearing designer may take care of an

external load value to get improved journal stability in case when journal mass is lower than the critical mass.

## 5. Conclusion

The present study investigates the influence of surface roughness patterns on the stability of symmetric two lobe non recessed hybrid journal bearing compensated with capillary restrictor. The dynamic behaviors of the bearing have been computed in terms of threshold



speed margin and critical journal mass to address the stability. The journal center motion trajectories have been obtained by solving the nonlinear equations of motion. Based on the simulated results of the study presented in the above section, the following conclusions have been drawn:

- i. The stability of two lobe symmetric hybrid journal bearing changes significantly as the value of surface roughness pattern parameter changes.
- ii. The nonlinear equation of journal motion predicts stable motion for longitudinal ( $\gamma = 6$ ) and isotropic ( $\gamma = 1$ ) surface roughness patterns, even though the  $\bar{M}_j = 1.1\bar{M}_c$  when the non circular journal bearing ( $\delta \geq 1.0$ ) operates at higher values of external load  $\bar{W}_0 = 4.0$ . The noteworthy observation also reveals that the transverse roughness pattern ( $\gamma = 1/6$ ) provides stable motion and other pattern ( $\gamma = 6, 1$ ) including smooth surface forms limit cycle motion, when  $\bar{M}_j = 1.1\bar{M}_c$  and  $\bar{W}_0 = 2.0$ .
- iii. When  $\bar{M}_j = \bar{M}_c$ , the nonlinear journal center motion trajectory provides stable motion for all the values of roughness pattern parameter except the transverse roughness pattern at  $\bar{W}_0 = 4.0$  and  $\delta = 1.20$ .
- iv. The nonlinear equation of journal center motion predicts higher safety margin for stability at the lower values of external load ( $\bar{W}_0 = 2.0$ ) than the higher values of an external load ( $\bar{W}_0 = 4.0$ ) when  $\bar{M}_j = 0.9\bar{M}_c$ .
- v. The bearing with offset factor more than one provides the largest value of threshold speed margin for longitudinal roughness pattern when  $\bar{M}_j = \bar{M}_c$ .
- vi. A proper selection of roughness pattern parameters and bearing geometry is essential to obtain the improved nonlinear journal center motion stability.

### Conflict of interest

The authors report no conflict of interest.

### Funding

This research received no specific grant from any funding agency in the public, commercial, or not-for-profit sectors.

### References

- Basavaraja J, Satish SC and Jain SC (2009) A study of misaligned roughened two-lobe hole-entry hybrid journal bearing. *Industrial Lubrication and Tribology* 61: 220–227.
- Boyver J, Fillon M and Pierre-Danos I (2007) Influence of wear on the behavior of a two-lobe hydrodynamic journal bearing subjected to numerous start ups and stops. *Journal of Tribology* 129: 205–208.
- Choy FK, Braun MJ and Hu Y (1992) Nonlinear transient and frequency response analysis of a hydrodynamic journal bearing. *Journal of Tribology* 114: 448–454.
- Christensen H (1969) Stochastic models for hydrodynamic lubrication of rough surfaces. *Proceedings of the Institution of Mechanical Engineers, Part I* 184: 1013–1026.
- Christensen H and Tonder K (1973) The hydrodynamic lubrication of rough journal bearings. *Journal of Lubrication Technology* 95: 166–172.
- Dowson D (1962) A generalized Reynolds equation for fluid film lubrication. *International Journal of Mechanical Engineering Sciences* 4: 159–170.
- Fayolle P and Childs DW (1999) Rotordynamic evaluation of a roughened-land hybrid bearing. *Journal of Tribology* 121: 133–138.
- Ghosh MK and Nagraj A (2004) Rotordynamic characteristics of a multilobe hybrid journal bearing in turbulent lubrication. *Proceedings of the Institution of Mechanical Engineers, Part J: Journal of Engineering Tribology* 218: 61–70.
- Ghosh MK and Satish MR (2003) Rotor dynamic characteristics of multi lobe hybrid bearings with short sills—part I. *Tribology International* 36: 625–632.
- Goenka PK and Booker JF (1983) Effect of surface ellipticity on dynamically loaded cylindrical bearing. *Journal of Lubrication Technology* 105: 1–12.
- Jagadeesha KM, Nagaraju T, Satish SC and Jain SC (2012) 3-D surface roughness effects on transient non-Newtonian response of dynamically loaded journal bearings. *Tribology Transactions* 55: 32–42.
- Khonsari MM (1990) The self-excited whirl orbits of a journal in a sleeve bearing lubricated with micropolar fluids. *Acta-Mechanica* 81: 235–244.
- Kushare PB and Satish SC (2013) A study of two lobe non recessed worn journal bearing operating with non-Newtonian lubricant. *Proceedings of the Institution of Mechanical Engineers, Part J: Journal of Engineering Tribology* 227: 1418–1437.
- Kushare PB and Satish SC (2014) Nonlinear transient stability study of two lobe symmetric hole entry worn hybrid journal bearing operating with non-Newtonian lubricant. *Tribology International* 69: 84–101.
- Leonard R and Rowe WB (1973) Dynamic force coefficients and the mechanism of instability in hydrostatic journal bearings. *Wear* 23: 277–282.
- Lin J-R (2007) Application of the Hopf bifurcation theory to limit cycle prediction of short journal bearings with isotropic roughness effects. *Proceedings of the Institution of Mechanical Engineers, Part J: Journal of Engineering Tribology* 221: 869–879.
- Lund JW (1987) Review of the concept of dynamic coefficients for fluid film bearings. *Journal of Tribology* 109: 37–41.
- Malik M, Bhargava SK and Sinhasan R (1989) The transient response of a journal in plane hydrodynamic bearing during acceleration and deceleration periods. *Tribology Transactions* 32: 61–69.
- Nagaraju T, Satish SC and Jain SC (2002) Influence of surface roughness effects on the performance of non recessed

- hybrid journal bearings. *Tribology International* 35: 467–487.
- Nagaraju T, Satish SC and Jain SC (2007) Influence of surface roughness on non-Newtonian thermo hydrostatic performance of a hole-entry hybrid journal bearing. *Journal of Tribology* 129: 595–602.
- Newkirk BL and Taylor HD (1925) Shaft whipping due to oil action in journal bearings. *General Electric Review* 28: 559–568.
- Patir N and Cheng HS (1978) An average flow model for determining effect of three-dimensional roughness on partial hydrodynamic lubrication. *Journal of Lubrication Technology* 100: 12–17.
- Patir N and Cheng HS (1979) Application of average flow model to lubrication between rough sliding surfaces. *Journal of Lubrication Technology* 101: 220–229.
- Phalle VM, Satish SC and Jain SC (2011) Influence of wear on the performance of a 2-lobe multirecess hybrid journal bearing system compensated with membrane restrictor. *Tribology International* 44: 380–395.
- Pinkus O (1956) Analysis of elliptical bearing. *ASME Transaction* 78: 965–973.
- Ramesh J, Majumdar BC and Rao NS (1995) Non-linear transient analysis of submerged oil journal bearings considering surface roughness and thermal effects. *Proceedings of the Institution of Mechanical Engineers, Part J: Journal of Engineering Tribology* 209: 53–61.
- San Andres L (1990) Turbulent hybrid bearings with fluid inertia effects. *Journal of Tribology* 112: 699–707.
- San Andres L (1997) Transient response of externally pressurized fluid film bearings. *Tribology Transaction* 40: 147–155.
- Satish SC, Phalle VM and Jain SC (2012) Performance of a noncircular 2-lobe multirecess hydrostatic journal bearing with wear. *Industrial lubrication and Tribology* 64: 171–181.
- Satish SC and Kushare PB (2015) Two lobe non-recessed roughened Hybrid journal bearing-A comparative study. *Tribology International* 83: 51–68.
- Schuller FT (1971) Experiments on the stability of water-lubricated three-lobe hydrodynamic journal bearings at zero load. *NASA Technical Note* 1–23.
- Sinhasan R and Goyal KC (1995) Transient Response of a Two-Lobe Journal Bearing Lubricated with Non-Newtonian Lubricant. *Tribology International* 28: 233–239.
- Turaga R, Sekhar AS and Majumdar BC (1999) Unbalance response and stability of a rotor supported on hydrodynamic journal bearings with rough surfaces. *Proceedings of the Institution of Mechanical Engineers, Part J: Journal of Engineering Tribology* 213: 31–34.
- Turaga R, Sekhar AS and Majumdar BC (2000) Non-linear transient stability analysis of a rigid rotor supported on hydrodynamic journal bearings with rough surfaces. *Tribology Transactions* 43: 447–452.
- Wang W, Yang L, Wang T and Yu L (2012) Nonlinear dynamic coefficients prediction of journal bearings using partial derivative method. *Proceedings of the Institution of Mechanical Engineers, Part J: Journal of Engineering Tribology* 226: 328–339.
- Yoshimoto S and Kikuchi K (1999) Step response characteristics of hydrostatic journal bearings with self-controlled restrictors employing a floating disk. *Journal of Tribology* 121: 315–320.
- Zhicheng P, Shuguo W, Qingming L and Wei C (1993) Theoretical and experimental study of the dynamic transient characteristics of a hydrostatic bearing. *Wear* 160: 27–31.